Calculating nonadiabatic couplings and Berry's phase by variational quantum eigensolvers

Shiro Tamiya,^{1,2,*} Sho Koh,^{3,†} and Yuya O. Nakagawa^{3,‡}

¹Department of Applied Physics, Graduate School of Engineering,
The University of Tokyo, 7-3-1 Hongo, Bynkyo-ku, Tokyo 113-8656, Japan

²Photon Science Center, Graduate School of Engineering,
The University of Tokyo, 7-3-1 Hongo, Bunkyo-ku, Tokyo 113-8656, Japan

³QunaSys Inc., Aqua Hakusan Building 9F, 1-13-7 Hakusan, Bunkyo, Tokyo 113-0001, Japan

(Dated: October 30, 2021)

The variational quantum eigensolver (VQE) is an algorithm to find eigenenergies and eigenstates of systems in quantum chemistry and quantum many-body physics. The VQE is one of the most promising applications of near-term quantum devices to investigate such systems. Here we propose an extension of the VQE to calculate the nonadiabatic couplings of molecules in quantum chemical systems and Berry's phase in quantum many-body systems. Both quantities play an important role to understand the properties of a system beyond the naive adiabatic picture, e.g., nonadiabatic dynamics and topological phase of matter. We provide quantum circuits and classical post-processings to calculate the nonadiabatic couplings and Berry's phase. Furthermore, we simulate the photodissociation dynamics of a lithium fluoride molecule using the nonadiabatic couplings evaluated on a real quantum device. Our proposal widens the applicability of the VQE and the possibility of near-term quantum devices to study molecules and quantum many-body systems.

I. INTRODUCTION

Quantum computers currently available or likely to be available in the near future are attracting growing attention. They are referred to as noisy intermediate-scale quantum (NISQ) devices [1], comprising tens or hundreds of qubits without quantum error correction. While it remains unclear whether they have "quantum advantage" over classical computers, the fact that they work explicitly based on the principle of quantum mechanics motivates researches on finding applications and developing quantum algorithms for practical problems that are classically intractable [2–8]. In particular, investigating quantum many-body systems with the variational quantum eigensolver (VQE) [9] is believed to be one of the most promising applications for NISQ devices [1].

The VQE is an algorithm to obtain eigenenergies and eigenstates of a given quantum Hamiltonian. In the VQE, quantum and classical computations are separated appropriately, and interactive quantum-classical hybrid architecture eases the difficulty of implementing the algorithm in the NISQ devices [9–14]. The VQE, which was originally proposed for finding the eigenenergy of the ground state, has been extended to find the excited energies and states [12, 15–20], non-equilibrium steady states [21, 22], derivatives of eigenenergies with respect to external parameters of the system [23, 24], and the Green's function [25].

This study aims to add a new recipe to the catalog of the VQE-based algorithms for quantum systems. We

propose a method to calculate the nonadiabatic couplings (NACs) [26, 27] of molecules in quantum chemistry and Berry's phase [28–30] of quantum many-body systems by utilizing the results of the VQE. Both quantities are related to the variation of slow degrees of freedom of the system and play a crucial role in the study of quantum chemistry, condensed matter physics, optics, and nuclear physics [29–35].

The NACs in quantum chemistry are defined as couplings between two different electronic states under the Born-Oppenheimer approximation [36], which are induced nonadiabatically by motions of nuclei (vibrations). They are fundamental in the nonadiabatic molecular dynamics simulations to study various interesting dynamical phenomena such as photochemical reactions around the conical intersection and electron transfers [31–34]. On the other hand, Berry's phase is defined as a phase acquired by an eigenstate when external parameters of a system are varied adiabatically along a closed path in the parameter space. It reflects intrinsic information about a system such as topological properties of materials. For example, several symmetry-protected topological phases are characterized by Berry's phase [37– 40. Berry's phase has become influential increasingly in many fields of modern physics, including condensed matter physics and high-energy physics [29, 30, 35].

Mathematically, the NACs and Berry's phase are related to derivatives of eigenstates with respect to external parameters of a system. In this study, in order to evaluate the NACs and Berry's phase based on the VQE, we develop analytical formulas and explicit quantum circuits to calculate the inner products related to the derivatives of the eigenstates. A naive way of calculation of the NACs based on the VQE requires the Hadamard test [41] with a lot of controlled operations, whereas our method replaces it with the measurements of expectation values

^{*} tamiya@qi.t.u-toyko.ac.jp

 $^{^{\}dagger}$ koh@qunasys.com

[‡] nakagawa@qunasys.com

of observables, which is tractable on NISQ devices compared to the Hadamard test. Our method for calculating Berry's phase still uses the Hadamard test at most once, which is the same as the previous study [42] simulating adiabatic dynamics. Nevertheless, by utilizing the definition of Berry's phase, we also carry out the calculation for Berry's phase based on the measurements of expectation values and remove any undesired dynamical phase contribution. Finally, we present the simulation of photodissociation dynamics of a lithium fluoride molecule with the value of the nonadiabatic couplings evaluated on the real quantum device, IBM Q Experience [43], by our proposed methods. Our results enlarge the possible scopes of the VQE algorithm and the NISQ devices for simulating various quantum systems.

The rest of the paper is organized as follows. We briefly review the definition of the NACs and Berry's phase in Sec. II. The VQE algorithm is also reviewed in Sec. III. Our main results are presented in Secs. IV and V, where we describe the ways to calculate the NACs and Berry's phase based on the VQE. The results of the experiment of estimating the nonadiabatic coupling using IBM Q hardware and the simulation of photodissociation dynamics with our methods are shown in Sec. VI. The discussion about the cost analysis for running our algorithms on quantum devices is provided in Sec. VII. We conclude our study in Sec. VIII. Further numerical demonstrations of our algorithms are provided in Supplemental Material [44].

II. REVIEW OF THE NONADIABATIC COUPLINGS AND BERRY'S PHASE

In this section, we review definitions of the NACs [26, 27] and Berry's phase [28].

Let us consider a quantum system which has external parameters $\vec{R}=(R_1,\ldots,R_{N_x})\in\mathbb{R}^{N_x}$. These parameters \vec{R} characterize the system, e.g., coordinates of nuclei in the case of quantum chemistry, electromagnetic field applied to a system in the case of conducting metals. We call \vec{R} as "system-parameters" and represent the Hamiltonian of the system which depends on \vec{R} by $H(\vec{R})$. The eigenvalues and eigenstates of $H(\vec{R})$ are denoted by $\{E_i(\vec{R})\}_i$ and $\{|\chi_i(\vec{R})\rangle\}_i$. We assume that $\{E_i(\vec{R})\}_i$ and $\{|\chi_i(\vec{R})\rangle\}_i$ depend on \vec{R} smoothly and that there is no degeneracy in the eigenspectrum unless explicitly stated in the text.

A. Nonadiabatic couplings

Here let us consider a molecular system and $H(\vec{R})$ as the electronic Hamiltonian. Definitions of the first-order NAC (1-NAC) d_{kl}^I and the second-order NAC (2-NAC)

 D_{kl}^{I} are as follows,

$$d_{kl}^{I}(\vec{R}) = \langle \chi_k(\vec{R}) | \frac{\partial}{\partial R_I} | \chi_l(\vec{R}) \rangle, \qquad (1)$$

$$D_{kl}^{I}(\vec{R}) = -\langle \chi_k(\vec{R}) | \frac{\partial^2}{\partial \vec{R}_{i}^2} | \chi_l(\vec{R}) \rangle, \qquad (2)$$

where k and l are different indices for eigenlevels and $l = 1, \ldots, N_x$ denotes the index for the system-parameters. The Hellman-Feynman theorem gives a simpler expression of the 1-NAC as

$$d_{kl}^{I} = -\frac{\langle \chi_k(\vec{R}) | \frac{\partial H}{\partial R_I} | \chi_l(\vec{R}) \rangle}{E_k(\vec{R}) - E_l(\vec{R})}, \tag{3}$$

which means that the 1-NAC becomes large when two eigenstates are close to degenerate ($E_k \sim E_l$). We take advantage of this expression when calculating the 1-NAC in Sec. IV. The 1-NAC is also called the vibronic coupling, and lies in the heart of various nonadiabatic molecular dynamics algorithms such as the Tully's fewest switches method [31, 32] and *ab initio* multiple spawning [45, 46].

Equation (2) in the case of k=l is related to the diagonal Born-Oppenheimer correction (DBOC) defined as

$$E_{\rm DBOC}(k) = -\sum_{\substack{\alpha = x, y, z}} \frac{1}{2M_m} \langle \chi_k(\vec{R}) | \frac{\partial^2}{\partial R_{m_\alpha}^2} | \chi_k(\vec{R}) \rangle,$$
(4)

where k is the eigenlevel to be considered, M_m is the mass of the nucleus m, and $R_{m_{\alpha}}$ is α -coordinate ($\alpha = x, y, z$) of the nucleus m. It is argued that this correction sometimes brings out crucial differences in stability and dynamics of molecules [47–50].

In addition, we comment on the gauge invariance of the NACs. Overall phase factors of eigenstates are arbitrary in general, so there is a $U(1)^M$ degree of freedom in the definition of the NACs,

$$|\chi_k(\vec{R})\rangle \to e^{i\Theta_k(\vec{R})} |\chi_k(\vec{R})\rangle,$$
 (5)

where $k=0,\ldots,M-1,\,M$ is the number of eigenlevels to be considered, and $\Theta_k(\vec{R}) \in \mathbb{R}$ is an arbitrary smooth function of \vec{R} . The 1-NAC (Eq. (1)) and the 2-NAC (Eq. (2)) are not invariant under the transformation (5). This invariance must be resolved in each algorithm utilizing the value of the NACs. For example, see Refs. [51–53]. We note that real-valued eigenfunctions are usually considered in quantum chemistry, but complex eigenfunctions may be obtained in the VQE in general.

B. Berry's phase

Berry's phase [28] is defined for a closed loop \mathcal{C} in the parameter space \mathbb{R}^{N_x} as,

$$\Pi_{\mathcal{C}} = -i \int_{\mathcal{C}} d\vec{R} \cdot \langle \chi_k(\vec{R}) | \frac{d}{d\vec{R}} | \chi_k(\vec{R}) \rangle, \qquad (6)$$

where $\int_{\mathcal{C}} \dots$ is the line integral along the closed loop \mathcal{C} , $|\chi_k(\vec{R})\rangle$ is the k-th eigenstate of the Hamiltonian $H(\vec{R})$. If one prepares the k-th eigenstate of the system $|\chi_k(\vec{R}_0)\rangle$ at some system-parameters \vec{R}_0 and adiabatically varies them in time along \mathcal{C} , the final state will obtain the phase $e^{-i\Pi_C}$ in addition to the dynamical phase.

We note that Berry's phase is always real by definition because the normalization condition $\langle \chi_k(\vec{R})|\chi_k(\vec{R})\rangle = 1$ leads to $\frac{d}{d\vec{R}}(\langle \chi_k(\vec{R})|\chi_k(\vec{R})\rangle) = 2 \mathrm{Re} \left(\langle \chi_k(\vec{R})|\frac{d}{d\vec{R}}|\chi_k(\vec{R})\rangle\right) = \vec{0}$. Moreover, if one can consider only real-valued functions as the eigenstate (this is the case for quantum chemistry problems without any electric/magnetic field or dissipation), Berry's phase vanishes because $\mathrm{Im} \left(\langle \chi_k(\vec{R})|\frac{d}{d\vec{R}}|\chi_k(\vec{R})\rangle\right) = \vec{0}$.

Finally, we point out the gauge invariance of Berry's phase. The eigenstates have U(1) gauge freedom stemming from arbitrariness of overall phases for them. Under U(1) gauge transformation (Eq. (5)), Berry's phase is invariant only up to an integer multiple of 2π . Since Berry's phase appears as $e^{-i\Pi_C}$, this arbitrariness does not affect the physics, and we can consider Berry's phase as an observable property of the system [29, 30, 35].

III. REVIEW OF VARIATIONAL QUANTUM EIGENSOLVER

In this section, we review the VQE algorithm [9] to obtain a ground state and excited states of a given Hamiltonian. We also describe how to compute analytical derivatives of optimal circuit-parameters of the VQE with respect to system-parameters of the Hamiltonian. Methods described in this section are repeatedly used in Secs. IV and V to calculate the 1- and 2-NACs and Berry's phase.

Again, let us consider an n-qubit quantum system whose Hamiltonian is $H(\vec{R})$. In the VQE, we introduce an ansatz quantum circuit $U(\vec{\theta})$ and the ansatz state $|\varphi_0(\vec{\theta})\rangle$ in the form of

$$|\varphi_0(\vec{\theta})\rangle = U(\vec{\theta}) |\psi_0\rangle,$$
 (7)

where $|\varphi_0\rangle$ is a reference state and $\vec{\theta}=(\theta_1,\ldots,\theta_{N_{\theta}})\in\mathbb{R}^{N_{\theta}}$ is a vector of circuit-parameters contained in the ansatz circuit. We assume $U(\vec{\theta})$ to be a product of unitary matrices each with one parameter,

$$U(\vec{\theta}) = U_N(\theta_N) \cdots U_2(\theta_2) U_1(\theta_1). \tag{8}$$

We also assume each unitary $U_a(\theta_a)$ consists of non-parametric quantum gates and parametric gates in the form of $e^{ig_aP_a\theta_a}$ generated by a Pauli product $P_a \in \{I,X,Y,Z\}^{\otimes n}$ with a coefficient $g_a \in \mathbb{R}$ $(a=1,\ldots,N_\theta)$. Note that many ansätze proposed in previous studies fall into this category [9, 11, 17, 54–58]. We will represent $U_j(\theta_j)\cdots U_i(\theta_i)$ as $U_{i:j}$ for simplicity.

A. Variational quantum eigensolver for ground state and excited states

The original VQE algorithm finds a ground state of a given Hamiltonian based on the variational principle of quantum mechanics. In the VQE, one optimizes the circuit-parameters $\vec{\theta}$ variationally by classical computers so that the expectation value

$$E_0(\vec{\theta}, \vec{R}) = \langle \varphi_0(\vec{\theta}) | H(\vec{R}) | \varphi_0(\vec{\theta}) \rangle \tag{9}$$

is minimized with respect to $\vec{\theta}$. When the circuitparameters $\vec{\theta}$ converge to optimal ones $\vec{\theta}^*$, we can expect the optimal state $|\varphi_0(\vec{\theta}^*)\rangle$ will be a good approximation to the ground state of $H(\vec{R})$. Since tasks of evaluation and optimization of quantum circuits are distributed to quantum and classical computers, it is easier to implement the algorithm on the near-quantum devices [9–14].

After the proposal of the original VQE algorithm, there are a variety of extensions of the VQE to find excited states of a given Hamiltonian [12, 15–20]. As we will see in Secs. IV and V, one has to compute (approximate) eigenenergies and transition amplitudes of several Pauli operators between obtained eigenstates to calculate the NACs. From this viewpoint, the most appropriate methods to calculate them are the subspace-search VQE (SSVQE) [16] algorithm and its cousin algorithm, the multistate contracted VQE (MCVQE) algorithm [17]. Here we briefly describe the SSVQE just for completeness, but formulas for the MCVQE are quite similar.

To obtain approximate eigenenergies and eigenstates up to $i=0,\ldots,M-1$, the SSVQE algorithm uses M easy-to-prepare orthonormal states $\{|\psi_i\rangle\}_{i=0}^{M-1}$ (e.g. computational basis) as reference states. For our algorithms to work, the reference states also have to be chosen so that we can readily prepare the superpositions of them on quantum devices. The SSVQE proceeds so as to minimize the following cost function,

$$\mathcal{L}_{\vec{R}}(\vec{\theta}) = \sum_{i=0}^{M-1} w_i \langle \psi_i | U^{\dagger}(\vec{\theta}) H(\vec{R}) U(\vec{\theta}) | \psi_i \rangle, \qquad (10)$$

where $\{w_i\}_{i=0}^{M-1}$ are positive and real weights which satisfy $w_0 > w_1 > \cdots > w_{M-1} > 0$. When the cost function converges to the minimum at $\vec{\theta}^*(\vec{R})$, it follows that

$$|\varphi_i(\vec{R})\rangle = U(\vec{\theta}^*(\vec{R})) |\psi_i\rangle,$$
 (11)

$$\tilde{E}_i(\vec{R}) = \langle \varphi_i(\vec{R}) | H(\vec{R}) | \varphi_i(\vec{R}) \rangle,$$
 (12)

are good approximations of the eigenstates and eigenenergies, respectively.

One of the most distinctive features of the SSVQE and the MCVQE algorithms is that one can readily compute transition amplitudes $\langle \varphi_k(\vec{R})|A|\varphi_l(\vec{R})\rangle$ of any observable A between the (approximate) eigenstates obtained. Although evaluation of the transition amplitude between two quantum states requires the Hadamard test in general, which contains a lot of extra and costly controlled

gates [59], the SSVQE and the MCVQE circumvent the difficulty by preparing superposition of two eigenstates. It is possible to evaluate the transition amplitude by low-cost quantum circuits without extra controlled gates as

$$\operatorname{Re}\left(\langle \varphi_{k}(\vec{R})|A|\varphi_{l}(\vec{R})\rangle\right)$$

$$=\frac{1}{2}\left(\langle \varphi_{k,l}^{+}(\vec{R})|A|\varphi_{k,l}^{+}(\vec{R})\rangle - \langle \varphi_{k,l}^{-}(\vec{R})|A|\varphi_{k,l}^{-}(\vec{R})\rangle\right),$$

$$\operatorname{Im}\left(\langle \varphi_{k}(\vec{R})|A|\varphi_{l}(R)\rangle\right)$$

$$=\frac{1}{2}\left(\langle \varphi_{k,l}^{i+}(\vec{R})|A|\varphi_{k,l}^{i+}(\vec{R})\rangle - \langle \varphi_{k,l}^{i-}(\vec{R})|A|\varphi_{k,l}^{i-}(\vec{R})\rangle\right),$$
(13)

where $|\varphi_{k,l}^{\pm}(\vec{R})\rangle = U(\vec{\theta}^*(\vec{R}))(|\psi_k\rangle \pm |\psi_l\rangle)/\sqrt{2}$ and $|\varphi_{k,l}^{i\pm}(\vec{R})\rangle = U(\vec{\theta}^*(\vec{R}))(|\psi_k\rangle \pm i\,|\psi_l\rangle)/\sqrt{2}$. Since each term of the right hand sides of the equation is an expectation value of the observable, the evaluation of the transition amplitude is tractable on near-term quantum devices.

B. Derivatives of optimal parameters

To calculate the NACs and Berry's phase with the result of the VQE on near-term quantum devices, we also need derivatives of the optimal circuit-parameters $\vec{\theta}^*(\vec{R})$ with respect to the system parameters \vec{R} . These derivatives are given by solving equations [23]

$$\sum_{b=1}^{N_{\theta}} \frac{\partial^{2} E_{0}(\vec{\theta}^{*}(\vec{R}), \vec{R})}{\partial \theta_{a} \partial \theta_{b}} \frac{\partial \theta_{b}^{*}(\vec{R})}{\partial R_{I}} = -\frac{\partial^{2} E_{0}(\vec{\theta}^{*}(\vec{R}), \vec{R})}{\partial \theta_{a} \partial R_{I}}, \quad (14)$$

$$\sum_{b=1}^{N_{\theta}} \frac{\partial^{2} E_{0}(\vec{\theta}^{*}(\vec{R}), \vec{R})}{\partial \theta_{a} \partial \theta_{b}} \frac{\partial^{2} \theta_{b}^{*}(\vec{R})}{\partial R_{I} \partial R_{J}} = -\gamma_{a}^{(IJ)}, \quad (15)$$

where

$$\gamma_c^{(IJ)} = \sum_{a,b} \frac{\partial^3 E_0(\vec{\theta}^*(\vec{R}), \vec{R})}{\partial \theta_c \partial \theta_a \partial \theta_b} \frac{\partial \theta_a^*}{\partial x_i} \frac{\partial \theta_b^*}{\partial x_j} \\
+ 2 \sum_a \frac{\partial^3 E_0(\vec{\theta}^*(\vec{R}), \vec{R})}{\partial \theta_c \partial \theta_a \partial R_J} \frac{\partial \theta_a^*}{\partial x_I} + \frac{\partial^3 E_0(\vec{\theta}^*(\vec{R}), \vec{R})}{\partial \theta_c \partial R_I \partial R_J}, \tag{16}$$

simultaneously for $a=1,\ldots,N_{\theta}$ (with $I,J=1,\ldots,N_{x}$ fixed). Now we use notations as follows:

$$\frac{\partial^2 E_0(\vec{\theta}^*(\vec{R}), \vec{R})}{\partial \theta_a \partial R_I} := \left. \frac{\partial^2 E_0(\vec{\theta}, \vec{R})}{\partial \theta_a \partial R_I} \right|_{\vec{\theta} = \vec{\theta}^*(\vec{R}), \vec{R} = \vec{R}}.$$
 (17)

The quantities appearing in Eq. (14) and Eq. (15), such as $\frac{\partial^2 E_0(\vec{\theta}^*(\vec{R}), \vec{R})}{\partial \theta_a \partial \theta_b}$ and $\frac{\partial^2 E_0(\theta^*(\vec{R}), \vec{R})}{\partial \theta_a \partial R_I}$, can be evaluated quantum circuits on near-term quantum devices using the method shown in Ref. [23]. Therefore one can solve Eq. (14) and Eq. (15) on classical computers and obtain the derivatives of the optimal circuit-parameters $\{\frac{\partial \theta_a^*(\vec{R})}{\partial R_I}, \frac{\partial \theta_a^*(\vec{R})}{\partial R_I \partial R_J}\}_{a=1}^{N_{\theta}}$.

IV. CALCULATING NONADIABATIC COUPLINGS WITH VARIATIONAL QUANTUM EIGENSOLVER

In this section, we explain how to calculate the 1-NAC and 2-NAC with the VQE.

A. First-order nonadiabatic coupling

Evaluation of the 1-NAC based on the VQE is simple by utilizing the formula (3). First, we perform the SSVQE or the MCVQE and obtain approximate eigenstates $|\varphi_i(\vec{R})\rangle$ and eigenenergies \tilde{E}_i of $H(\vec{R})$. Then we calculate the derivative of the Hamiltonian, $\frac{\partial H}{\partial R_I}$, on classical computers. This step can be done numerically as well as analytically [23, 24]. Finally, evaluating the transition amplitude $\langle \varphi_k(\vec{R})|\frac{\partial H}{\partial R_I}|\varphi_l(\vec{R})\rangle$ on quantum devices by using the method of Eq. (13) and substituting it into Eq. (3) gives the value of the 1-NAC.

B. Second-order nonadiabatic coupling

Next, we introduce an analytical evaluation method of the 2-NAC on near-term quantum devices.

After obtaining approximate eigenstates $\{|\varphi_i(\vec{R})\rangle\}_i$ by the SSVQE or the MCVQE, putting them into Eq. (2) yields

$$\langle \varphi_{k}(\vec{R}) | \frac{\partial^{2}}{\partial R_{I}^{2}} | \varphi_{l}(\vec{R}) \rangle$$

$$= \sum_{a,b} \frac{\partial \theta_{a}^{*}}{\partial R_{I}} \frac{\partial \theta_{b}^{*}}{\partial R_{I}} \langle \varphi_{k} | \partial_{a} \partial_{b} \varphi_{l} \rangle + \sum_{c} \frac{\partial^{2} \theta_{c}^{*}}{\partial R_{I}^{2}} \langle \varphi_{k} | \partial_{c} \varphi_{l} \rangle,$$
(18)

where we denote $\frac{\partial}{\partial \theta_a} \frac{\partial}{\partial \theta_b} |\varphi_j\rangle$ and $\frac{\partial}{\partial \theta_c} |\varphi_j\rangle$ as $|\partial_a \partial_b \varphi_j\rangle$ and $|\partial_c \varphi_j\rangle$, respectively. We note that plugging Eq. (18) when k = l into Eq. (4) gives the formula of the DBOC based on the VQE.

The derivatives of the optimal circuit-parameters such as $\frac{\partial \theta_a^*}{\partial R_I}$ and $\frac{\partial^2 \theta_c^*}{\partial R_I^2}$ can be calculated by the method reviewed in Sec. III. The terms $\langle \varphi_k | \partial_a \partial_b \varphi_l \rangle$ and $\langle \varphi_k | \partial_c \varphi_l \rangle$ can be evaluated with the Hadamard test [41] in a naive way, but its implementation is costly for near-term quantum devices. Therefore, in the following, we describe how to reduce the evaluation of $\langle \varphi_k | \partial_a \partial_b \varphi_l \rangle$ and $\langle \varphi_k | \partial_c \varphi_l \rangle$ to the measurements of the expectation value of observables, which is the standard process of the near-term quantum algorithms.

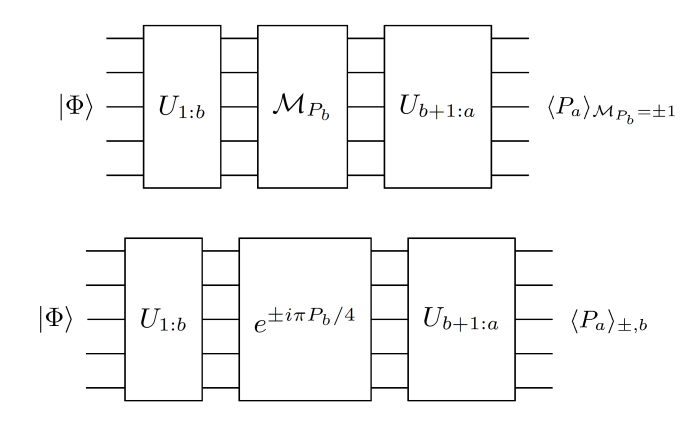


FIG. 1. Quantum circuits to evaluate Eq. (21) (top) and Eq. (24) (bottom), respectively. \mathcal{M}_{P_b} is a projective measurement of the Pauli operator P_b .

1. Evaluation of $\langle \varphi_k | \partial_a \partial_b \varphi_l \rangle$

To calculate $\langle \varphi_k | \partial_a \partial_b \varphi_l \rangle$, let us first consider evaluating

$$\langle \Phi | U^{\dagger}(\vec{\theta}) \frac{\partial}{\partial \theta_a} \frac{\partial}{\partial \theta_b} U(\vec{\theta}) | \Phi \rangle$$
 (19)

with $|\Phi\rangle$ being an arbitrary reference state. When a=b, it follows $\langle \Phi | U^{\dagger}(\vec{\theta}) \frac{\partial^2}{\partial \theta_a^2} U(\vec{\theta}) | \Phi \rangle = -g_a^2 \langle \Phi | U^{\dagger}(\vec{\theta}) U(\vec{\theta}) | \Phi \rangle = -g_a^2$. When $a \neq b$, we assume $1 \leq b < a \leq N_\theta$ without loss of generality. By using the method in Ref. [59], the real and imaginary parts of Eq. (19) are evaluated separately in the following way.

The real part is calculated with quantum circuits containing projective measurements of the Pauli operator P_b denoted by \mathcal{M}_{P_b} ,

$$\operatorname{Re}\left(\langle \Phi | U^{\dagger}(\vec{\theta}) \frac{\partial}{\partial \theta_{a}} \frac{\partial}{\partial \theta_{b}} U(\vec{\theta}) | \Phi \rangle\right)$$

$$= -g_{a}g_{b} \times$$

$$\left(p(\mathcal{M}_{P_{b}} = 1) \langle P_{a} \rangle_{\mathcal{M}_{P_{b}} = 1} - p(\mathcal{M}_{P_{b}} = -1) \langle P_{a} \rangle_{\mathcal{M}_{P_{b}} = -1}\right),$$
(20)

where

$$\langle P_a \rangle_{\mathcal{M}_{P_b} = \pm 1}$$

$$= \frac{1}{4} \frac{\langle \Phi | U_{1:b}^{\dagger} (I \pm P_b) U_{b+1:a}^{\dagger} P_a U_{b+1:a} (I \pm P_b) U_{1:b} | \Phi \rangle}{p(\mathcal{M}_{P_b} = \pm 1)}$$
(21)

is the conditional expectation value of P_a when the projective measurement of P_b yields ± 1 , and

$$p(\mathcal{M}_{P_b} = \pm 1) = \left| \frac{1}{2} (I \pm P_b) U_{1:b} \left| \Phi \right\rangle \right|^2$$
 (22)

is the probability of getting the result ± 1 for the projective measurement of P_b . If P_b is a single Pauli operator or even if P_b is a multi-qubit Pauli operator, we expect that the projective measurement of it can be performed in near-term quantum devices [60]. The total circuit for evaluating Eq. (21) is shown in the top panel of Fig. 1.

On the other hand, the imaginary part of Eq. (19) can be calculated as

$$\operatorname{Im}\left(\langle \Phi | U^{\dagger}(\vec{\theta}) \frac{\partial}{\partial \theta_{a}} \frac{\partial}{\partial \theta_{b}} U(\vec{\theta}) | \Phi \rangle\right)$$

$$= \frac{g_{a}g_{b}}{2} (\langle P_{a} \rangle_{+,b} - \langle P_{a} \rangle_{-,b}),$$
(23)

where

$$\langle P_a \rangle_{\pm,b}$$

= $\langle \Phi | U_{1:b}^{\dagger} e^{\mp i\pi P_b/4} U_{b+1:a}^{\dagger} P_a U_{b+1:a} e^{\pm i\pi P_b/4} U_{1:b} | \Phi \rangle (24)$

is the expectation value of P_a for the quantum state $U_{b+1:a}e^{\pm i\pi P_b/4}U_{1:b}|\Phi\rangle$. The circuit for calculation is shown in the bottom panel of Fig 1.

Then, to obtain $\langle \varphi_k | \partial_a \partial_b \varphi_l \rangle$ we take advantage of the following equality

$$2 \langle \varphi_{k} | \partial_{a} \partial_{b} \varphi_{l} \rangle = \langle \varphi_{k,l}^{+} | \partial_{a} \partial_{b} \varphi_{k,l}^{+} \rangle - \langle \varphi_{k,l}^{-} | \partial_{a} \partial_{b} \varphi_{k,l}^{-} \rangle + \frac{1}{i} \left(\langle \varphi_{k,l}^{i+} | \partial_{a} \partial_{b} \varphi_{k,l}^{i+} \rangle - \langle \varphi_{k,l}^{i-} | \partial_{a} \partial_{b} \varphi_{k,l}^{i-} \rangle \right),$$
(25)

where $|\varphi_{k,l}^{\pm}\rangle = U_{1:N}(|\psi_k\rangle \pm |\psi_l\rangle)/\sqrt{2}$ and $|\varphi_{k,l}^{i\pm}\rangle = U_{1:N}(|\psi_k\rangle \pm i |\psi_l\rangle)/\sqrt{2}$. All terms in the right hand side of (25) can be evaluated by the method described above with taking $|\Phi\rangle$ appropriately, so the $\langle \varphi_k | \partial_a \partial_b \varphi_l \rangle$ is also obtained.

2. Evaluation of $\langle \varphi_k | \partial_c \varphi_l \rangle$

Next, we describe how to compute $\langle \varphi_k | \partial_c \varphi_l \rangle$. It follows that

$$\langle \varphi_k | \partial_c \varphi_l \rangle = \langle \psi_k | U^{\dagger}(\vec{\theta}) \frac{\partial}{\partial \theta_c} U(\vec{\theta}) | \psi_l \rangle$$

$$= i g_c \langle \psi_k | U_{1:c}^{\dagger} P_c U_{1:c} | \psi_l \rangle.$$
(26)

The term in the last line can be evaluated by the method of Eq. (13) by substituting $|\varphi_{k,l}^{\pm}(\vec{R})\rangle$ by $U_{1:c}\frac{1}{\sqrt{2}}(|\psi_k\rangle\pm|\psi_l\rangle)$ and $|\varphi_{k,l}^{\pm i}(\vec{R})\rangle$ with $U_{1:c}\frac{1}{\sqrt{2}}(|\psi_k\rangle\pm i\,|\psi_l\rangle)$.

3. Summary

In summary, calculation of the 2-NAC D_{kl}^{I} proceeds as follows:

1. Perform the SSVQE or the MCVQE and obtain approximate eigenstates $|\varphi_i(\vec{R})\rangle$ and eigenenergies $\tilde{E}_i(\vec{R})$ of $H(\vec{R})$.

- 2. Calculate the derivative of the Hamiltonian $\frac{\partial H}{\partial R_I}$ on classical computers and obtain $\frac{\partial \theta_a^*}{\partial R_I}$ and $\frac{\partial^2 \theta_c^*}{\partial R_I^2}$ in Eq. (18) by solving Eq. (14) and Eq. (15).
- 3. For all $a, b = 1, ..., N_{\theta}$, evaluate Eq. (19) for $|\Phi\rangle = |\varphi_{k,l}^{\pm}\rangle, |\varphi_{k,l}^{i\pm}\rangle$, by using Eq. (20) and Eq. (23). Plugging them in Eq. (25) yields the value of $\langle \varphi_k | \partial_a \partial_b \varphi_l \rangle$.
- 4. For all $c = 1, ..., N_{\theta}$, evaluate $\langle \varphi_k | \partial_c \varphi_l \rangle$ according to Eq. (26).
- 5. Substituting all values obtained in previous steps into Eq. (18) gives the 2-NAC.

V. CALCULATING BERRY'S PHASE WITH VARIATIONAL QUANTUM EIGENSOLVER

In this section, we describe a method for calculating Berry's phase with the VQE algorithm. Our method is based on evaluating the integrand of the definition of Berry's phase (6) based on the VQE and numerical integration of it. The ambiguity of an overall phase of the eigenstate plays a crucial role in our setup, and one Hadamard test is needed to fix the phase and calculate Berry's phase in general. In the following, without loss of generality, we only consider the ground state as the eigenstate.

Let us change the variable of integration from the system-parameters \vec{R} to the (optimized) circuitparameters $\vec{\theta}^*$ and see where the ambiguity comes in. We consider performing the VQE from one point \vec{R}_0 of the closed loop \mathcal{C} in the system-parameters space and continue doing it along \mathcal{C} . Here we can expect that $\vec{\theta}^*(\vec{R})$ are the smooth functions along C. However, the value of the optimal parameters θ^* at the starting point of \mathcal{C} and the ending point of C can be different from each other. In other words, the optimal parameters $\vec{\theta}^*$ do not form the closed loop in the circuit-parameter space even when \mathcal{C} is the closed loop in the system-parameter space. This is because the VQE does not care about the overall phase of the ground state, and for most cases there is a redundancy in the ansatz $|\varphi_0(\vec{\theta})\rangle$ such that $|\varphi_0(\vec{\theta}_1)\rangle = e^{i\xi} |\varphi_0(\vec{\theta}_2)\rangle, e^{i\xi} \neq 1 \text{ for some } \vec{\theta}_1 \neq \vec{\theta}_2.$

To take into account this redundancy, we introduce the reference ground state $|\phi_0(\vec{R})\rangle$ which is single-valued over the closed loop \mathcal{C} . The relationship between $|\phi_0(\vec{R})\rangle$ and the result of the VQE is written as

$$|\phi_0(\vec{R}_0)\rangle = e^{i\Theta_{s(t)}} |\varphi_0(\vec{\theta}^*(\vec{R}_0)_{s(t)})\rangle, |\phi_0(\vec{R})\rangle = e^{i\Theta(\vec{R})} |\varphi_0(\vec{\theta}^*(\vec{R}))\rangle \quad (\vec{R} \neq \vec{R}_0),$$
(27)

where $\vec{\theta}^*(\vec{R}_0)_s$ and $\vec{\theta}^*(\vec{R}_0)_t$ are optimal circuit-parameters at the start \vec{R}_0 and the end \vec{R}_0 of the closed

loop, respectively, and $\Theta \in \mathbb{R}$ is a phase factor. The definition of Berry's phase (6) can be transformed as

$$\Pi_{\mathcal{C}} = -i \int_{\mathcal{C}} d\vec{R} \cdot \langle \phi_0(\vec{R}) | \frac{\partial}{\partial \vec{R}} | \phi_0(\vec{R}) \rangle
= -i \int_{\mathcal{C}'} d\vec{\theta} \cdot \langle \varphi_0(\vec{\theta}) | \frac{\partial}{\partial \vec{\theta}} | \varphi_0(\vec{\theta}) \rangle \Big|_{\vec{\theta} = \vec{\theta}^*(\vec{R})} + (\Theta_t - \Theta_s),$$
(28)

where C' is the path $\{\vec{\theta}^*(\vec{R})|\vec{R} \in C\}$ in the circuitparameter space. In the following, we explain how to evaluate the terms in the right hand side of Eq. (28).

A. Evaluation of the first term

The first term of Eq. (28) is computed by discretization of the closed loop \mathcal{C} and numerical integration of the integrand. We discretize the value of the system-parameters \vec{R} on \mathcal{C} as $\vec{R}_0, \ldots, \vec{R}_{K-1}$ appropriately and also define $\vec{R}_K = \vec{R}_0$. The VQE algorithm is performed for all points $\{\vec{R}_p\}_{p=0}^K$ and the optimal circuit-parameters are obtained as $\{\vec{\theta}_p^* = \vec{\theta}^*(\vec{R}_p)\}_{p=0}^K$. We note that $\vec{\theta}_0 = \vec{\theta}^*(\vec{R}_0)_s$ and $\vec{\theta}_K = \vec{\theta}^*(\vec{R}_0)_t$. The integrand of the line integral on \mathcal{C}' is

$$\langle \varphi_{0}(\vec{\theta}) | \frac{\partial}{\partial \theta_{a}} | \varphi_{0}(\vec{\theta}) \rangle \bigg|_{\vec{\theta} = \vec{\theta}^{*}(\vec{R})} = \langle \psi_{0} | U^{\dagger}(\vec{\theta}^{*}) \frac{\partial}{\partial \theta_{a}} U(\vec{\theta}^{*}) | \psi_{0} \rangle$$
$$= ig_{a} \langle \psi_{0} | U^{\dagger}_{1:a} P_{a} U_{1:a} | \psi_{0} \rangle, \tag{29}$$

so it is evaluated by measuring the expectation value of P_a for the state $U_{1:a} | \psi_0 \rangle$. Therefore the line integral is approximated by

$$\int_{\mathcal{C}'} d\vec{\theta} \cdot \langle \varphi_0(\vec{\theta}) | \frac{\partial}{\partial \vec{\theta}} | \varphi_0(\vec{\theta}) \rangle \bigg|_{\vec{\theta} = \vec{\theta}^*(\vec{R})}$$

$$\approx \sum_{p=0}^{K-1} (\vec{\theta}_{p+1} - \vec{\theta}_p) \cdot \langle \varphi_0(\vec{\theta}) | \frac{\partial}{\partial \vec{\theta}} | \varphi_0(\vec{\theta}) \rangle \bigg|_{\vec{\theta} = \vec{\theta}_p^*} . \quad (30)$$

B. Evaluation of $\Theta_t - \Theta_s$

The second term in Eq. (28), $\Theta_{\rm t} - \Theta_{\rm s}$, is evaluated by the difference of the overall phase of two wavefunctions $|\varphi(\theta_0^*)\rangle$ and $|\varphi(\theta_K^*)\rangle$. This can be performed by estimating $\langle \varphi(\theta_0^*)|\varphi(\theta_K^*)\rangle = e^{i(\Theta_{\rm t}-\Theta_{\rm s})}$ with the Hadamard test [41] depicted in Fig. 2. We note that it requires one ancillary qubit and the controlled- $U(\vec{\theta})$ gates, which are costly for near-term quantum devices.

However, there are several possible situations where we can avoid the Hadamard test. One such case is to use the ansatz that has no ambiguity, i.e., $|\varphi_0(\vec{\theta}_1)\rangle \propto |\varphi_0(\vec{\theta}_2)\rangle \Rightarrow |\varphi_0(\vec{\theta}_1)\rangle = |\varphi_0(\vec{\theta}_2)\rangle$ holds for all $\vec{\theta}_1, \vec{\theta}_2$. In this case, the phase difference does not appear in the expression of Berry's phase (28). Another case is to use the

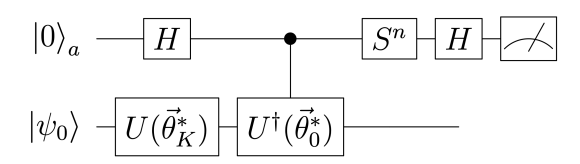


FIG. 2. The Hadamard test to evaluate the phase difference $\Theta_{\rm t}-\Theta_{\rm s}$ in Eq. (28). The measurement for the ancillary qubit gives the value of ${\rm Re}\left(\langle \varphi(\vec{\theta}_0^*)|\varphi(\vec{\theta}_K^*)\rangle\right)$ and ${\rm Im}\left(\langle \varphi(\vec{\theta}_0^*)|\varphi(\vec{\theta}_K^*)\rangle\right)$ for n=0,1.

collective VQE method [61], which optimizes the parameters $\vec{\theta}(\vec{R})$ simultaneously for all \vec{R} , with imposing some penalty for the path C' to be closed and thereby no phase difference to appear.

C. Comparison with previous studies

We here compare previous work on calculating Berry's phase on quantum devices with our method. In Ref. [42], Berry's phase is calculated by simulating adiabatic dynamics of the system $U_{\mathcal{C}} = \mathcal{T}e^{-i\int_0^T ds H(s)}$, where \mathcal{T} is the time-ordered product and H(s) is a time-dependent Hamiltonian, which varies along the closed loop \mathcal{C} in sufficiently long time T. $U_{\mathcal{C}}$ is implemented on quantum computers by the Suzuki-Trotter decomposition, and the Hadamard test like Fig. 2 is performed to detect the phase difference between the initial ground state $|\chi(\vec{R}_0)\rangle$ and the time-evolved state $U_c(\vec{R}_0)\rangle$. phase difference between $|\chi(\vec{R}_0)\rangle$ and $U_c |\chi(\vec{R}_0)\rangle$ contains the dynamical phase and Berry's phase, but the former phase can be neglected by combining the forward- and backward-time evolutions by assuming the Hamiltonian of the system has the time-reversal symmetry. Compared with this strategy, our proposal for calculating Berry's phase based on the VQE has two features. First, we do not have to assume the time-reversal symmetry in the system to remove the contribution from the dynamical phase like in the previous study because we directly calculate Berry's phase based on the definition Eq. (6). Our method can apply to general quantum systems. Second, the causes of errors are quite different. More concretely, while the errors in the previous methods arise from the Trotterization of the time evolution operator, the errors in our method mainly come from two sources: one is the approximation error of the eigenstates obtained by the VQE, and the other is the numerical error of integration in Eq. (30). These errors can be reduced by deepening the ansatz circuits and taking more discretized points on \mathcal{C} , respectively. We comment that further research is needed to conclude the difference in the performance between our method and these previous methods.

Finally, we introduce another method to calculate

Berry's phase based on the VQE with a lot of Hadamard tests. Using the formula

$$\Pi_{\mathcal{C}} \approx -i \sum_{i=0}^{K} \operatorname{Im} \left(\ln \langle \varphi_0(\vec{\theta}_i^*) | \varphi_0(\vec{\theta}_{i+1}^*) \rangle \right), \qquad (31)$$

with taking the principal branch of the complex logarithm, $-\pi \leq \operatorname{Im}(z) < \pi$ for $z \in \mathbb{C}$, is one of the candidates for avoiding discretization error of the closed loop \mathcal{C} and numerical instability [62]. The value of $\langle \varphi_0(\vec{\theta}_i^*) | \varphi_0(\vec{\theta}_{i+1}^*) \rangle$ is evaluated by the Hadamard test in Fig. 2 by substituting $\vec{\theta}_{0(K)}^*$ with $\vec{\theta}_{i(i+1)}^*$.

D. Summary

Berry's phase can be calculated based on the VQE as follows:

- 1. Discretize the closed loop \mathcal{C} in the systemparameters space as $\{\vec{R}_p\}_{p=0}^K$ appropriately and perform the VQE for all points. The optimal circuit-parameters for \vec{R}_p are denoted as $\vec{\theta}^*(\vec{R}_p)$.
- 2. Calculate the first term of Eq. (28) by using Eq. (29) and Eq. (30).
- 3. If necessary, evaluate the phase difference $\Theta_{\rm t}-\Theta_{\rm s}$ by the Hadamard test shown in Fig. 2.
- 4. Substituting all values obtained in the previous steps into Eq. (28) gives the Berry's phase.

VI. EXPERIMENT ON A REAL QUANTUM DEVICE

In this section, we show an experimental result of our algorithm for the 1-NAC on a real quantum device and the non-adiabatic molecular dynamics (MD) simulation based on the experimental values of the 1-NAC.

We consider a lithium fluoride (LiF) molecule with bond length R and its electronic states under the Born-Oppenheimer approximation. In this system, the potential energy curves, or eigenenergies E as a function of R, of the two lowest ${}^{1}\Sigma^{+}$ states are known to exhibit the avoided crossing [65–68], and it plays a crucial role for nonadiabatic dynamics such as photo-disassociation. Here we focus on this avoided crossing and the resulting nonadiabaitc dynamics by modeling the system with a simple two-state model. Specifically, the electronic Hamiltonian of LiF at bond distance R is constructed by two orbitals obtained by the state-average complete active space self-consistent field (CASSCF) method [69]. By considering symmetries in the system, one can obtain a two-qubit Hamiltonian $H_{LiF}(R)$ from that electronic Hamiltonian. Further details are described in Appendix A.

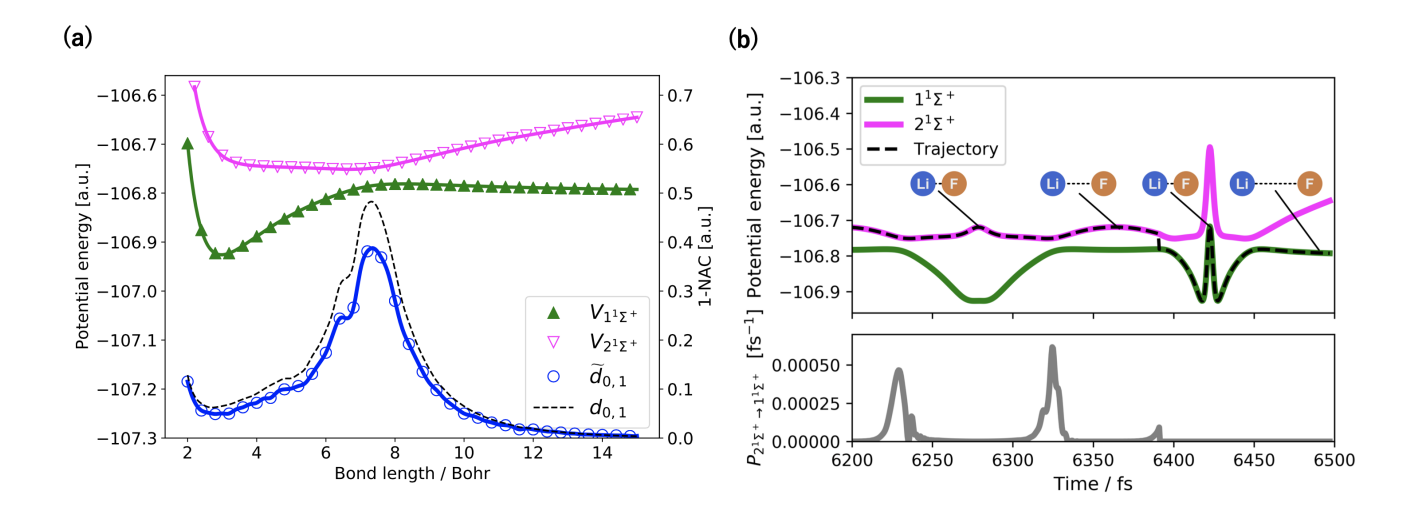


FIG. 3. (a) Numerical results of the potential energy curves of the $1^1\Sigma^+$ state (upper triangles) and $2^1\Sigma^+$ state (lower triangles) obtained by the SSVQE and experimental results of the 1-NAC $\tilde{d}_{0,1}$ between the two states (circles) at the bond distance R in the range of 2 to 15 Å. The solid lines represent the spline interpolated curves computed by SciPy, a numerical library in Python [63]. The dashed lines show the exact numerical results of the 1-NAC $d_{0,1}$ in a noiseless situation calculated with the Qiskit's statevector simulator [64]. The exact potential energy curves calculated by the exact diagonalization are not presented in the figure since they coincide with the ones obtained by the SSVQE (presented in the figure) by less than 10^{-10} a.u for the whole range of R. (b) Potential energies of $1^1\Sigma^+$ state and $2^1\Sigma^+$ state (upper panel) and the transition probability $P_{2^1\Sigma^+\to 1^1\Sigma^+}$ (lower panel) for one trajectory obtained by the TSH molecular dynamics simulation. On this trajectory, the molecule hops from $2^1\Sigma^+$ state to $1^1\Sigma^+$ state during bond shrinking motion at 6391.0 fs and it disassociates into Li and F atoms.

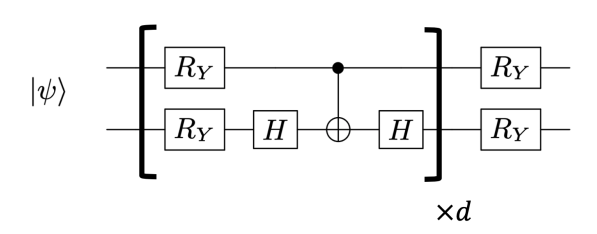


FIG. 4. The ansatz circuit $U(\vec{\theta})$ for the SSVQE. Each $R_Y = \exp(-iY\theta/2) = \begin{pmatrix} \cos\theta/2 & \sin\theta/2 \\ -\sin\theta/2 & \cos\theta/2 \end{pmatrix}$ has a rotational angle θ as an independent parameter, and d=4 denotes the depth of the ansatz. The rotation angles of R_Y gates are optimized during the SSVQE in our experiments. We note that quantum states generated by this circuit for real wavefunction $|\psi\rangle$ remain real for any choice of θ .

We run our algorithm to calculate the 1-NAC (Sec. IV) of $H_{\rm LiF}(R)$ at various bond length R in the IBM Q cloud quantum device (ibmq_valencia) [43]. First, the SSVQE calculation for $H_{\rm LiF}(R)$ is performed on a classical simulator where the exact and noiseless expectation values of observables are obtained. The ansatz for the SSVQE, $U(\vec{\theta})$, is depicted in Fig. 4 and we optimize the parameters $\vec{\theta}$ to minimize the cost function (10). The initial states to which the ansatz applied are $|\psi_0\rangle = |00\rangle, |\psi_1\rangle = |01\rangle$ states. To calculate

the singlet (S=0) states ${}^{1}\Sigma^{+}$, we penalize the triplet (S=1) states by modifying the Hamiltonian in the cost function as $H' = H_{LiF}(R) + \beta \hat{S}^2$, where \hat{S}^2 is the spin squared operator and $\beta = 4.0$ is a constant. We obtain the (approximate) eigenstates $|\varphi_{0,1}(\vec{\theta}^*)\rangle = U(\vec{\theta}^*) |\psi_{0,1}\rangle$ and eigenenergies $\tilde{E}_{0,1}$ for two $^{1}\Sigma^{+}$ states in this way from the classical simulator (Fig. 3(a) shows the potential energy curves). Next, the transition amplitude $\langle \varphi_0(\vec{\theta}^*) | \frac{dH_{\mathrm{LiF}}(R)}{dR} | \varphi_1(\vec{\theta}^*) \rangle$ is computed on a quantum device by evaluating each term of the right hand sides of Eq. (13) with 8192 shots. Since the wavefunction is real by definition of the ansatz $U(\vec{\theta})$, we consider only the real part of Eq. (13). Finally, the 1-NAC in Eq. (3) is calculated by substituting the numerator with and doing the denominator with $\tilde{E}_0 - \tilde{E}_1$. We comment that the way of calculating the 1-NAC here is chosen to remove the effect of the noise and errors in the real quantum device during the SSVQE and focus on evaluating the transition amplitude.

The result of the 1-NAC is shown in Fig. 3(a). Because of the noise in the real quantum device, the values of the transition amplitude are smaller than the exact results but still qualitatively consistent with them. This shrinking could be resolved by, for example, using the error mitigation technique [70, 71] for near-term quantum devices.

In addition, we perform the trajectory surface hopping (TSH) [72] molecular dynamics calculation using

Tully's fewest switches algorithm [31] based on the obtained values of the potential energy curves and the 1-NAC (Fig. 3(a)). We assume a situation where a LiF molecule is excited by light to the first electronic excited state. The initial bond length of LiF is taken as the equilibrium bond length R_0 of the electronic ground state $1^{1}\Sigma^{+}$ on the first electronic excited state $2^{1}\Sigma^{+}$. The initial kinetic energy of nuclei is set to be the same as the zero-point vibration energy of $1^{1}\Sigma^{+}$ which is obtained by vibrational frequency analysis under harmonic oscillator approximation. In the TSH simulation, the nuclear energy gradient $\frac{\partial \tilde{E}_{0,1}}{\partial R}$ and the 1-NAC at a various bond length R are requested by the TSH program code, and we feed it with the values interpolated from the results of the SSVQE and the 1-NAC experiment. The details of the interpolation are described in Appendix B. We run one trajectory with a time step of 0.5 fs and present the trajectory hops from $2^{1}\Sigma^{+}$ to $1^{1}\Sigma^{+}$ where the disassociation occurs as shown in Fig. 3(b). Since the two-state model we adopted gives a relatively large gap (~ 0.98 eV) at the crossing point, the hoppings are rarely observed, but our results show the potential that TSH can be performed with the near-term quantum devices. The TSH simulation is conducted by the open-source library SHARC [73–75].

Although we consider the 1-NAC throughout this section, we perform additional numerical demonstrations of our methods by simulating the quantum circuits to calculate the 1-NAC and 2-NAC of the hydrogen molecules and Berry's phase of a two-site spin model in Supplemental Material.

VII. DISCUSSION

Our proposed methods presented in the previous sections are based on the analytical derivative of the eigenstates obtained by the SSVQE. This section compares our methods with those using the numerical derivative of the eigenstates by the finite difference method. The comparison will be made from two points of view: (1) the number of distinct Hamiltonians to perform the SSVQE to obtain the optimal circuit-parameters $\vec{\theta}^*$ and (2) the total number of measurements required to evaluate the NACs and Berry's phase after performing the SSVQE. We ignore the cost of classical computation throughout analyses in this section.

We recall that N_{θ} and N_x are the dimensions of the circuit-parameters and system-parameters, respectively. The number of qubits in the system is denoted as n and the number of Pauli terms in the Hamiltonian as N_H . For quantum chemistry problems N_H is typically $O(n^4)$ [2, 3], but several methods for reducing N_H are proposed [76, 77]. The detailed derivations of the formulas in this section (Eqs. (32)(34)(37)) are presented in Appendix C.

A. Cost of 1-NAC

Let us consider our proposed method to calculate the 1-NAC d_{kl}^I with fixed k, l and all $I = 1, ..., N_x$ at some fixed system-parameters \vec{R} . The evaluation of the 1-NAC is performed by calculating the denominator and numerator in Eq. (3). Both can be obtained by applying a single optimized ansatz circuit $U(\vec{\theta}^*(\vec{R}))$ resulting from the SSVQE to several initial states and measuring appropriate observables, so the number of distinct Hamiltonians to perform the SSVQE is just one. Meanwhile, the number of measurements to calculate the 1-NAC is estimated as follows. When we write the Hamiltonian as H(R) = $\sum_{i=1}^{N_H} h_i(\vec{R}) P_i$, where P_i is Pauli operator and $h_i(\vec{R})$ is a real coefficient, the values of $\langle \varphi_{k(l)} | H(\vec{R}) | \varphi_{k(l)} \rangle =$ $\sum_{i=1}^{N_H} h_i(\vec{R}) \left< \varphi_{k(l)} | P_i | \varphi_{k(l)} \right>$ and $\left< \varphi_k | \partial H(\vec{R}) / \partial R_I | \varphi_l \right> = \sum_{i=1}^{N_H} \partial h_i(\vec{R}) / \partial R_I \left< \varphi_k | P_i | \varphi_l \right>$ are necessary to compute the 1-NAC. The term $\left< \varphi_{k(l)} | P_i | \varphi_{k(l)} \right>$ is evaluated as the expectation value of P_i , and similarly the term $\langle \varphi_k | P_i | \varphi_l \rangle$ $(i=1,\ldots,N_H)$ is evaluated as a sum of four expectation values in the right hand sides of Eq. (13). By taking into account errors in evaluating those expectations values, the number of measurements to estimate the 1-NAC within the error ϵ is given by

$$N_{\text{total}}^{\text{1-NAC}} = O\left[\frac{N_H}{\epsilon^2 |\Delta E_{k,l}|^4} \left(|\Delta E_{k,l}| \left\|\frac{\partial H}{\partial R_{I^*}}\right\| + \|H\||A_{I^*}|\right)^2\right], \tag{32}$$

where $A_I(\Delta E_{k,l})$ is the numerator (denominator) of Eq. (3), $||H|| = \sum_i |h_i|$, $||\partial H/\partial R_I|| = \sum_i |\partial h_i/\partial R_I|$, and $I^* = \operatorname{argmax}_I \left(|\Delta E_{k,l}| \left\|\frac{\partial H}{\partial R_I}\right\| + ||H|||A_I|\right)$. It scales with the number of the Pauli terms in the Hamiltonian but does not depend on the number of circuit-parameters N_θ by virtue of Eq. (3). The dependence on I, or the system-parameters, is also absent because it is absorbed into the classical computation of the coefficient $\partial h_i(\vec{R})/\partial R_I$ [23].

To compare with our method, one can consider a method to evaluate the 1-NAC based on numerical differentiation of the eigenstates obtained by the SSVQE. In such approach, the 1-NAC can be evaluated by the following formula.

$$d_{k,l}^{I} \approx \frac{\tau_{k,l}(\vec{R}, \vec{R} + h\vec{e}_{I}) - \tau_{k,l}(\vec{R}, \vec{R} - h\vec{e}_{I})}{2h},$$
 (33)

where $\tau_{k,l}(\vec{R}, \vec{R} \pm h\vec{e}_I) = \langle \varphi_k(\vec{\theta}^*(\vec{R})) | \varphi_l(\vec{\theta}^*(\vec{R} \pm h\vec{e}_I)) \rangle$, h is a positive number, and \vec{e}_I is the unit vector in I-th direction. For simplicity, we will represent $\tau_{k,l}(\vec{R}, \vec{R} \pm h\vec{e}_I)$ as $\tau_{k,l}^{\pm,I}$.

When evaluating each term of Eq. (33), we assume that $\tau_{k,l}^{\pm,I}$ is estimated from the overlap $\left| \langle \psi_k | U^{\dagger}(\vec{\theta}^*(\vec{R})) U(\vec{\theta}^*(\vec{R} \pm h\vec{e}_I) | \psi_l \rangle \right|^2$, which can be easily

evaluated from measurements on near-term quantum devices if $|\psi_k\rangle$, $|\psi_l\rangle$ are computational basis states [19]. We then obtain the value of $\tau_{k,l}^{\pm,I}$ by taking the square root of the overlaps with a positive sign (real value) [6]. This treatment can be justified when we solve problems in quantum chemistry, where wavefunctions are often real, and we adopt an ansatz which produces a real wavefunction. This approach to evaluate Eq. (33) avoids the costly Hadamard test and is considered to be feasible on near-term quantum devices. We note that our methods are always applicable without the assumption above.

To evaluate the 1-NAC with Eq. (33), we need optimal parameters $\vec{\theta}^*(\vec{R})$, $\vec{\theta}^*(\vec{R} \pm h\vec{e}_I)$ for all I, so the number of distinct Hamiltonians to perform the SSVQE in the finite difference method is $2N_x + 1 = O(N_x)$. By considering the error in estimating the overlaps, the number of measurements to estimate the 1-NAC with the precision of ϵ in the finite difference method is at least

$$N'_{\text{total}}^{\text{1-NAC}} = O(N_x/T_{k,l}^2 \epsilon^2), \tag{34}$$

where $T_{k,l} = \min_{\sigma=\pm,I} \tau_{k,l}^{\sigma,I}$ and we assume the condition $M_3 \geq O(\epsilon)$, where $M_3 = \max_I \max_{s \in [-h,h]} \left| \tau_{k,l}^{(I,3)}(s) \right|$ and $\tau_{k,l}^{(I,3)}(s) = \frac{d^3}{ds^3} \tau_{k,l} (\vec{R}, \vec{R} + s\vec{e}_I)$. Both our method (32) and the finite difference method (34) scale with ϵ^{-2} , so the prefactors determine the efficiency of them. When N_x , or the number of system-parameters (nuclei of the molecule), becomes large, the finite difference method will suffer from a large number of the SSVQE runs and the measurements compared with our method.

B. Cost of 2-NAC

To calculate the 2-NAC D_{kl}^{I} with fixed k,l and all $I=1,\ldots N_x$ at \vec{R} with our method, we require one optimized circuit-parameter $\theta^*(\vec{R})$, so the number of distinct Hamiltonians to perform the SSVQE is again one. Let us consider the number of measurements. We need the derivatives $\{\frac{\partial \theta_a^*}{\partial R_I}, \frac{\partial^2 \theta_a^*}{\partial R_I^2}\}_{I=1}^{N_x}$ which are obtained as the solutions of Eqs. (14)(15). The coefficients of these equations are determined within error ϵ by performing $O(N_{\theta}^3 N_H/\epsilon^2)$ measurements. Since the error propagation from the coefficients to the solutions $\left\{\frac{\partial \theta^*}{\partial R_I}, \frac{\partial^2 \theta^*}{\partial R_I^2}\right\}_{I=1}^{N_x}$ is very complicated, we here let the error of the solutions be ϵ (see Ref. [23] for similar discussion). The value of $\langle \varphi_k | \partial_a \partial_b \varphi_l \rangle$ $(a, b = 1, \dots, N_\theta)$ in Eq. (25) is obtained by measuring $O(N_{\theta}^2/\epsilon^2)$ times within error ϵ . Similarly, $\langle \varphi_k | \partial_c \varphi_l \rangle$ $(c = 1, ..., N_\theta)$ in Eq. (26) is calculated by $O(N_{\theta}/\epsilon^2)$ measurements. Therefore, the total number of measurements to evaluate the 2-NAC by our method is roughly given by

$$N_{\text{total}}^{2\text{-NAC}} = O(N_{\theta}^3 N_H / \epsilon^2), \tag{35}$$

where the meaning of ϵ has to be cared for. It does not depend on the number of system-parameters N_x .

The finite difference method is based on the following formula:

$$D_{k,l}^{I} \approx \frac{\tau_{k,l}(\vec{R}, \vec{R} + h\vec{e}_{I}) + \tau_{k,l}(\vec{R}, \vec{R} - h\vec{e}_{I})}{h^{2}}$$
 (36)

where we used $\tau_{k,l}(\vec{R}, \vec{R}) = 0$. Similarly to the case of the 1-NAC, the number of distinct Hamiltonians to perform the SSVQE is $O(N_x)$. To bound the error of the 2-NAC by ϵ , the finite difference method requires at least

$$N_{\text{total}}^{'2\text{-NAC}} = O\left(N_x^2/T_{k,l}^2 \epsilon^2\right)$$
 (37)

measurements under the condition $M_4 \geq O(\epsilon)$, where $M_4 = \max_I \max_{s \in [-h,h]} \left| \tau_{k,l}^{(I,4)}(s) \right|$ and $\tau_{k,l}^{(I,4)}(s) = \frac{d^4}{ds^4} \tau_{k,l}(\vec{R}, \vec{R} + s\vec{e}_I)$. The number of measurements in our method (35) does not depends on N_x while the finite difference method (37) does, as with the 1-NAC.

C. Cost of Berry's phase

For calculating Berry's phase, the closed path $\mathcal C$ is discretized into K points. The integrand (Eq. (28)) is evaluated at all K points and numerically integrated both in our method and the finite difference method. We therefore compare our method with the finite difference method only in terms of the cost to obtain the integrand at all the discretized points.

In our method, the integrand at each discretized point can be evaluated by Eq. (29). The total number of distinct Hamiltonians to perform the VQE is K+1=O(K). If we bound the error in estimating each integrand by ϵ , the total number of measurements is given by

$$N_{\text{total}}^{\text{Berry}} = O(KN_{\theta}/\epsilon^2).$$
 (38)

In the finite difference, the integrand can be evaluated with the finite difference method by the following formula.

$$\frac{\langle \varphi_0(\vec{R}_k) | \varphi_0(\vec{R}_k + h\vec{v}_k) \rangle - \langle \varphi_0(\vec{R}_k) | \varphi_0(\vec{R}_k - h\vec{v}_k) \rangle}{2h}$$
(39)

where $\vec{v}_k \propto \vec{R}_{k+1} - \vec{R}_k$ is the unit vector along the closed loop C. The minimal number of measurements to obtain all integrands within error ϵ can be derived in a similar way for the 1-NAC, and the result is

$$N'_{\text{total}}^{\text{Berry}} = O(K/T_{0,0}^2 \epsilon^2),$$
 (40)

VIII. CONCLUSION

In this paper, we have proposed methods to calculate the NACs and Berry's phase based on the VQE. We utilize the SSVQE and the MCVQE algorithms, which enable us to evaluate transition amplitudes of observables between approximate eigenstates. We explicitly present quantum circuits and classical post-processings to evaluate the NACs and Berry's phase in the framework of the VQE. For the 1-NAC, the calculations are simplified by taking advantage of the formula (3). The 2-NAC is obtained by combining the projective measurements and the expectation-value measurements of Pauli operators. The evaluation of Berry's phase is also carried out by the measurements of expectation values of Pauli operators with numerical integration of the definition of Berry's phase and does not suffer from the dynamical phase. To show the potential feasibility of our method for the 1-NAC on a near-term quantum device, we evaluate the value of the 1-NAC of a lithium fluoride molecule on the IBM Q processor. Based on those results, we perform the nonadiabatic molecular dynamics simulation of photo dissociation of a lithium fluoride for the first time. The methods given in the present paper contribute to enlarging the usage of the VQE and accelerate further developments to investigate quantum chemistry and quantum many-body problems on near-term quantum devices.

ACKNOWLEDGEMENT

This work is supported by MEXT Quantum Leap Flagship Program (MEXT Q-LEAP) Grant No. JP-MXS0118067394. A part of this work was performed for Council for Science, Technology and Innovation (CSTI), Cross-ministerial Strategic Innovation Promotion Program (SIP), "Photonics and Quantum Technology for Society 5.0" (Funding agency: QST). ST is supported by CREST (Japan Science and Technology Agency) JP-MJCR1671 and QunaSys Inc. YON acknowledges Takao Kobayashi for inspiring discussion to bring this project out. YON and ST acknowledge valuable discussions with Kosuke Mitarai and Wataru Mizukami. We acknowledge IBM Q Startup program for providing access to IBM Q cloud computers which are used in our experiment. A part of the numerical simulations in this work were done on Microsoft Azure Virtual Machines provided through the program Microsoft for Startups.

Appendix A: Hamiltonian for LiF

The model Hamiltonian of a LiF molecule at a bond length R under the Born-Oppenheimer approximation, $H_{\text{LiF}}(R)$, is constructed by the following steps. (1) The state-average CASSCF method with the active space of (6 orbital, 6 electrons) is carried out by adopting the aug-ccppvdz basis set. The state-average is taken for two

lowest ${}^{1}\Sigma^{+}$ states. (2) We pick two lowest σ, σ^{*} molecular orbitals from the six optimized orbitals of CASSCF and construct a fermionic Hamiltonian by using them. (3) The parity mapping method [78, 79] is employed to map the fermionic Hamiltonian to the qubit Hamiltonian; the number of qubits required is four at this point. Two qubits among the four are frozen from the symmetry constraints for the number of electrons and the number of total z-component of the spin [80], which finally results in the two-qubit Hamiltonian. The construction of the Hamiltonian is processed by PySCF [81] and Open-Fermion [82].

Appendix B: Interpolation of the results to perform TSH

As described in Sec. VI, we interpolate the values of the (approximate) eigenenergies \tilde{E}_0, \tilde{E}_1 and the 1-NAC $\tilde{d}_{0,1}$ evaluated at the finite number of points and supply them to the programming code for the TSH molecular dynamics simulation. Sixty-six points in the range of 2 to $15\mathring{A}$ are used for evaluation, and we perform the cubic spline interpolation for them implemented in Scipy, a numerical library in Python [63].

Appendix C: Cost analysis of our algorithms

Cost of our algorithm for 1-NAC

To estimate the number of measurements to evaluate the 1-NAC with our method, let us consider the error in estimating expectation values of the Hamiltonian $H(\vec{R})$ and $\frac{\partial H(\vec{R})}{\partial R}$. We write $H(\vec{R}) = \sum_{i=1}^{N_H} h_i(\vec{R}) P_i$ and $\frac{\partial H(\vec{R})}{\partial R} = \sum_{i=1}^{N_H} \frac{\partial h_i(\vec{R})}{\partial R} P_i$ as the same in the main text. The Hoeffding's inequality [83] implies that an expectation value $\langle P_i \rangle$ can be estimated within the precision ϵ_P with high probability $1 - \delta$ by measuring P_i for $O(\log(1/\delta)/\epsilon_P^2)$ times. When we perform $O(\log(1/\delta)/\epsilon_P^2)$ measurements for estimating each $\langle P_i \rangle$, the total error in estimating the expectation value of $H(\vec{R})$ is

$$\left| \widetilde{\langle H(\vec{R}) \rangle} - \langle H(\vec{R}) \rangle \right| \le \epsilon_P \sum_{i=1}^{N_H} |h_i| = \epsilon_P ||H||, \quad (C1)$$

where $\widetilde{\cdots}$ is an estimated value of \cdots and ||H|| = $\sum_{i=1}^{N_H} |h_i|$. In the same way, the error of $\langle \frac{\partial H(\vec{R})}{\partial R_I} \rangle$ is given

$$\left| \left\langle \frac{\partial H(\vec{R})}{\partial R_I} \right\rangle - \left\langle \frac{\partial H(\vec{R})}{\partial R_I} \right\rangle \right| \le \epsilon_P \left\| \frac{\partial H}{\partial R_I} \right\|, \quad (C2)$$

where $\|\partial H/\partial R_I\| = \sum_{i=1}^{N_H} |\partial h_i/\partial R_I|$. By using Eqs. (C1)(C2), we can derive the total number of measurements needed to estimate the 1-NAC within error ϵ . Equation (3) is evaluated in our method as

$$d_{k,l}^{I} = -\frac{\langle \varphi_{k,l}^{+} | \frac{\partial H(\vec{R})}{\partial R_{I}} | \varphi_{k,l}^{+} \rangle - \langle \varphi_{k,l}^{-} | \frac{\partial H(\vec{R})}{\partial R_{I}} | \varphi_{k,l}^{-} \rangle}{\langle \varphi_{k} | H(\vec{R}) | \varphi_{k} \rangle - \langle \varphi_{l} | H(\vec{R}) | \varphi_{l} \rangle}. \quad (C3)$$

When we perform $O(\log(1/\delta)/\epsilon_P^2)$ measurements to estimate the expectation value of each P_i appearing in $\langle \varphi_{k,l}^{\pm} | \frac{\partial H(\vec{R})}{\partial \vec{R}_I} | \varphi_{k,l}^{\pm} \rangle$, $\langle \varphi_{k(l)} | H(\vec{R}) | \varphi_{k(l)} \rangle$, the error propagation follows that the total error is given by

$$\left| \widetilde{d_{k,l}^I} - d_{k,l}^I \right| \lesssim \frac{2\epsilon_P}{|\Delta E_{k,l}|^2} \left(|\Delta E_{k,l}| \left\| \frac{\partial H}{\partial R_I} \right\| + \|H\| |A_I| \right), \tag{C4}$$

where A_I , $\Delta E_{k,l}$ are the numerator and denominator of Eq. (C3), respectively. To upper bound the error of $d_{k,l}^I$ by ϵ , it is enough to set

$$\epsilon_{P,I} = \frac{\epsilon |\Delta E_{k,l}|^2}{2\left(|\Delta E_{k,l}| \left\|\frac{\partial H}{\partial R_I}\right\| + \|H\||A_I|\right)}.$$
 (C5)

Recalling that the 1-NACs for all $I = 1, ..., N_x$ are obtained by the same results of the measurements $\langle P_i \rangle$, we conclude that the total number of measurements to estimate all the 1-NACs within the error ϵ with probability $1 - \delta$ is given by

 $N_{\rm total}^{1-{
m NAC}}$

$$= O\left[\frac{N_H \log(1/\delta)}{\epsilon^2 |\Delta E_{k,l}|^4} \left(|\Delta E_{k,l}| \left\| \frac{\partial H}{\partial R_{I^*}} \right\| + \|H\| |A_{I^*}| \right)^2\right], \tag{C6}$$

where $I^* = \operatorname{argmax}_I \left(|\Delta E_{k,l}| \left\| \frac{\partial H}{\partial R_I} \right\| + \|H\| |A_I| \right)$.

2. Cost of the finite difference method for 1-NAC

Let us discuss the number of measurements to calculate the 1-NAC with the finite difference method based on Eq. (33). Let $s_{k,l}^{\pm,I}$ denote the overlap $\left|\langle\psi_k|U^\dagger(\vec{\theta}^*(\vec{R}))U(\vec{\theta}^*(\vec{R}\pm h\vec{e}_I)|\psi_l\rangle\right|^2$ and we compute $\tau_{k,l}^{\pm,I}$ in Eq. (33) as $\tau_{k,l}^{\pm,I}=\sqrt{s_{k,l}^{\pm,I}}$. By using Hoeffding's inequality, we know that $O(\log(1/\delta)/\epsilon_s^2)$ projective measurements for the state $U^\dagger(\vec{\theta}^*(\vec{R}))U(\vec{\theta}^*(\vec{R}\pm h\vec{e}_I)|\psi_l\rangle$ onto the computational basis state $|\psi_k\rangle$ is required to estimate $s_{k,l}^{\pm,I}$ within error ϵ_s with probability $1-\delta$.

When the error of the overlap $s_{k,l}^{\pm,I}$ is bounded by ϵ_s , or $\left|\widetilde{s_{k,l}^{\pm,I}} - s_{k,l}^{\pm,I}\right| \leq \epsilon_s$, it follows that

$$\left| \widetilde{\tau_{k,l}^{\pm,I}} - \tau_{k,l}^{\pm,I} \right| \lesssim \frac{\epsilon_s}{2\tau_{\star}^{\pm,I}}.$$
 (C7)

The error of the 1-NAC with the finite difference method is then be expressed as

$$\left| d_{k,l}^{I} - \frac{\widetilde{\tau_{k,l}^{+,I}} - \widetilde{\tau_{k,l}^{-,I}}}{2h} \right| \le \frac{h^2}{6} M_3^{(I)} + \frac{\epsilon_s}{2h\tau_{k,l}^{I}}, \tag{C8}$$

where $\tau_{k,l}^I = \min\{\tau_{k,l}^{+,I}, \tau_{k,l}^{-,I}\}, M_3^{(I)} = \max_{s \in [-h,h]} \left|\tau_{k,l}^{(I,3)}(s)\right| \text{ and } \tau_{k,l}^{(I,3)}(s) = \frac{d^3}{ds^3}\tau_{k,l}(\vec{R}, \vec{R} + s\vec{e}_I).$ To upper bound the right-hand side by ϵ , we have to choose ϵ_s as

$$\epsilon_s = 2\tau_{k,l}^I \left(\epsilon h - \frac{h^3}{6} M_3^{(I)}\right). \tag{C9}$$

Therefore, the total number of measurements needed to evaluate the 1-NAC for all $I = 1, ..., N_x$ within the precision ϵ with the finite difference method is

$$N_{\text{total}}^{'1\text{-NAC}} = O \left[\frac{N_x \log(1/\delta)}{T_{k,l}^2 \left(\epsilon h - \frac{h^3}{6} M_3\right)^2} \right],$$
 (C10)

where $T_{k,l}^2 = \min_I \tau_{k,l}^I$ and $M_3 = \max_I M_3^{(I)}$. Moreover, to clarify the dependence of ϵ , we take h such that ϵ_s attains the maximum with respect to h and that $N_{\text{total}}^{'1\text{-NAC}}$ takes the minimum. This is realized for $h = \sqrt{\frac{2\epsilon}{M_3}}$ and we obtain $\epsilon_{s,\max} = \frac{4\sqrt{2}}{3}T_{k,l}M_3^{-\frac{1}{2}}\epsilon^{\frac{3}{2}}$. Under the assumption that $M_3 \geq O(\epsilon)$, we have $\epsilon_{s,\max} \leq \frac{4\sqrt{2}}{3}T_{k,l}\epsilon$. In such case, it follows that

$$N_{\text{total}}^{'\text{1-NAC}} = O\left(\frac{N_x \log(1/\delta)}{T_{k,l}^2 \epsilon^2}\right).$$
 (C11)

3. Cost of the finite difference method for 2-NAC

The same argument applies to the error of 2-NAC with the finite difference method based on Eq. (36). When we have $\left|\widetilde{\tau_{k,l}^{\pm,I}} - \tau_{k,l}^{\pm,I}\right| \leq \epsilon_s/(2\tau_{k,l}^{\pm,I})$, the error of Eq. (36) is given by

$$\left| D_{k,l}^{I} - \frac{\widetilde{\tau_{k,l}^{+}} + \widetilde{\tau_{k,l}^{-}}}{h^{2}} \right| \le \frac{h^{2}}{12} M_{4}^{(I)} + \frac{\epsilon_{s}}{h^{2} \tau_{k,l}^{I}}, \quad (C12)$$

where $M_4^{(I)} = \max_{s \in [-h,h]} \left| \tau_{k,l}^{(I,4)}(s) \right|$ and $\tau_{k,l}^{(I,4)}(s) = \frac{d^4}{ds^4} \tau_{k,l}(\vec{R}, \vec{R} + s\vec{e}_I)$. To suppress the error of the 2-NAC within ϵ with the finite difference method, we have to take ϵ_s as

$$\epsilon_s = \tau_{k,l}^I \left(\epsilon h^2 - \frac{h^4}{12} M_4^{(I)} \right), \tag{C13}$$

and obtain

where $M_4 = \max_I M_4^{(I)}$. Similarly to the analysis for the 1-NAC, when we take $h = \sqrt{\frac{3\epsilon}{M_4}}$, we obtain $\epsilon_{s,\max} = \frac{9}{8} \frac{\epsilon^2}{M_4}$. If $M_4 \geq O(\epsilon)$, it follows $\epsilon_{s,\max} \leq \frac{9}{8}\epsilon$. Finally, we reach

$$N'_{\text{total}}^{'2\text{-NAC}} = O\left(\frac{N_x^2 \log(1/\delta)}{T_{k,l}^2 \epsilon^2}\right).$$
 (C15)

- $N_{\text{total}}^{'2\text{-NAC}} = O\left[\frac{N_x^2}{T_{k,l}^2 \left(\epsilon h^2 \frac{h^4}{12} M_4\right)^2}\right],$ (C14)
- [1] J. Preskill, Quantum 2, 79 (2018).
- [2] S. McArdle, S. Endo, A. Aspuru-Guzik, S. Benjamin, and X. Yuan, arXiv:1808.10402 (2018).
- [3] Y. Cao, J. Romero, J. P. Olson, M. Degroote, P. D. Johnson, M. Kieferová, I. D. Kivlichan, T. Menke, B. Peropadre, N. P. D. Sawaya, S. Sim, L. Veis, and A. Aspuru-Guzik, Chemical Reviews 119, 10856 (2019).
- [4] K. Mitarai, M. Negoro, M. Kitagawa, and K. Fujii, Phys. Rev. A 98, 032309 (2018).
- [5] E. Farhi and H. Neven, arXiv:1802.06002 (2018).
- [6] V. Havlíček, A. D. Córcoles, K. Temme, A. W. Harrow, A. Kandala, J. M. Chow, and J. M. Gambetta, Nature 567, 209 (2019).
- [7] T. Kusumoto, K. Mitarai, K. Fujii, M. Kitagawa, and M. Negoro, arXiv:1911.12021 (2019).
- [8] E. Farhi, J. Goldstone, and S. Gutmann, arXiv preprint arXiv:1411.4028 (2014).
- [9] A. Peruzzo, J. McClean, P. Shadbolt, M.-H. Yung, X.-Q. Zhou, P. J. Love, A. Aspuru-Guzik, and J. L. O'Brien, Nature Communications 5, 4213 (2014).
- [10] P. J. J. O'Malley, R. Babbush, I. D. Kivlichan, J. Romero, J. R. McClean, R. Barends, J. Kelly, P. Roushan, A. Tranter, N. Ding, B. Campbell, Y. Chen, Z. Chen, B. Chiaro, A. Dunsworth, A. G. Fowler, E. Jeffrey, E. Lucero, A. Megrant, J. Y. Mutus, M. Neeley, C. Neill, C. Quintana, D. Sank, A. Vainsencher, J. Wenner, T. C. White, P. V. Coveney, P. J. Love, H. Neven, A. Aspuru-Guzik, and J. M. Martinis, Phys. Rev. X 6, 031007 (2016).
- [11] A. Kandala, A. Mezzacapo, K. Temme, M. Takita, M. Brink, J. M. Chow, and J. M. Gambetta, Nature 549, 242 (2017).
- [12] J. I. Colless, V. V. Ramasesh, D. Dahlen, M. S. Blok, M. E. Kimchi-Schwartz, J. R. McClean, J. Carter, W. A. de Jong, and I. Siddiqi, Phys. Rev. X 8, 011021 (2018).
- [13] C. Hempel, C. Maier, J. Romero, J. McClean, T. Monz, H. Shen, P. Jurcevic, B. P. Lanyon, P. Love, R. Babbush, A. Aspuru-Guzik, R. Blatt, and C. F. Roos, Phys. Rev. X 8, 031022 (2018).
- [14] A. Kandala, K. Temme, A. D. Córcoles, A. Mezzacapo, J. M. Chow, and J. M. Gambetta, Nature 567, 491 (2019).
- [15] J. R. McClean, M. E. Kimchi-Schwartz, J. Carter, and W. A. de Jong, Phys. Rev. A 95, 042308 (2017).
- [16] K. M. Nakanishi, K. Mitarai, and K. Fujii, Phys. Rev. Research 1, 033062 (2019).
- [17] R. M. Parrish, E. G. Hohenstein, P. L. McMahon, and T. J. Martínez, Phys. Rev. Lett. 122, 230401 (2019).
- [18] T. Jones, S. Endo, S. McArdle, X. Yuan, and S. C. Benjamin, Phys. Rev. A 99, 062304 (2019).

- [19] O. Higgott, D. Wang, and S. Brierley, Quantum 3, 156 (2019).
- [20] P. J. Ollitrault, A. Kandala, C.-F. Chen, P. K. Barkoutsos, A. Mezzacapo, M. Pistoia, S. Sheldon, S. Woerner, J. Gambetta, and I. Tavernelli, arXiv:1910.12890 (2019).
- [21] N. Yoshioka, Y. O. Nakagawa, K. Mitarai, and K. Fujii, arXiv:1908.09836 (2019).
- [22] H.-Y. Liu, Y.-C. Wu, G.-C. Guo, and G.-P. Guo, arXiv:2001.02552 (2020).
- [23] K. Mitarai, Y. O. Nakagawa, and W. Mizukami, Phys. Rev. Research 2, 013129 (2020).
- [24] R. M. Parrish, E. G. Hohenstein, P. L. McMahon, and T. J. Martinez, arXiv:1906.08728 (2019).
- [25] S. Endo, I. Kurata, and Y. O. Nakagawa, Phys. Rev. Research 2, 033281 (2020).
- [26] B. Lengsfield and D. R. Yarkony, Adv. Chem. Phys 82, 1 (1992).
- [27] D. R. Yarkony, Chemical Reviews 112, 481 (2012).
- [28] M. V. Berry, Proceedings of the Royal Society of London. A. Mathematical and Physical Sciences 392, 45 (1984).
- [29] D. Xiao, M.-C. Chang, and Q. Niu, Rev. Mod. Phys. 82, 1959 (2010).
- [30] E. Cohen, H. Larocque, F. Bouchard, F. Nejadsattari, Y. Gefen, and E. Karimi, Nature Reviews Physics 1, 437 (2019).
- [31] J. C. Tully, The Journal of Chemical Physics 93, 1061 (1990).
- [32] J. C. Tully, The Journal of Chemical Physics 137, 22A301 (2012).
- [33] I. Tavernelli, Accounts of Chemical Research 48, 792 (2015).
- [34] K. Takatsuka, T. Yonehara, K. Hanasaki, and Y. Arasaki, Chemical Theory beyond the Born-Oppenheimer Paradigm (WORLD SCIENTIFIC, 2015).
- [35] M. Nakahara, Geometry, topology and physics (CRC Press, 2003).
- [36] M. Born and R. Oppenheimer, Annalen der Physik 389, 457 (1927).
- [37] J. K. Asbóth, L. Oroszlány, and A. Pályi, A short course on topological insulators (Springer, 2016).
- [38] Y. Hatsugai, Journal of the Physical Society of Japan 75, 123601 (2006).
- [39] T. Kariyado, T. Morimoto, and Y. Hatsugai, Phys. Rev. Lett. 120, 247202 (2018).
- [40] H. Araki, T. Mizoguchi, and Y. Hatsugai, Phys. Rev. Research 2, 012009 (2020).
- [41] R. Cleve, A. Ekert, C. Macchiavello, and M. Mosca, Proceedings of the Royal Society A: Mathematical, Physical and Engineering Sciences (1997).

- [42] B. Murta, G. Catarina, and J. Fernández-Rossier, Phys. Rev. A 101, 020302 (2020).
- [43] "IBM Quantum Experience," (2020), https://quantum-computing.ibm.com/.
- [44] See Supplemental Material for details on additional numerical demonstrations of our methods by simulating the quantum circuits to calculate the NACs of the hydrogen molecules and Berry's phase of a two-site spin model.
- [45] M. Ben-Nun, J. Quenneville, and T. J. Martínez, The Journal of Physical Chemistry A 104, 5161 (2000).
- [46] M. Ben-Nun and T. J. Martínez, "Ab initio quantum molecular dynamics," in *Advances in Chemical Physics* (John Wiley & Sons, Ltd, 2002) pp. 439–512.
- [47] N. C. Handy, Y. Yamaguchi, and H. F. Schaefer, The Journal of Chemical Physics 84, 4481 (1986).
- [48] E. F. Valeev and C. D. Sherrill, The Journal of Chemical Physics 118, 3921 (2003).
- [49] I. G. Ryabinkin, L. Joubert-Doriol, and A. F. Izmaylov, The Journal of Chemical Physics 140, 214116 (2014).
- [50] R. Gherib, L. Ye, I. G. Ryabinkin, and A. F. Izmaylov, The Journal of Chemical Physics 144, 154103 (2016).
- [51] L. F. Errea, L. Fernández, A. Macías, L. Méndez, I. Rabadán, and A. Riera, The Journal of Chemical Physics 121, 1663 (2004).
- [52] Á. Vibók, G. J. Halász, S. Suhai, and M. Baer, The Journal of Chemical Physics 122, 134109 (2005).
- [53] G. Miao, N. Bellonzi, and J. Subotnik, The Journal of Chemical Physics 150, 124101 (2019).
- [54] B. T. Gard, L. Zhu, G. S. Barron, N. J. Mayhall, S. E. Economou, and E. Barnes, npj Quantum Information 6, 10 (2020).
- [55] J. Lee, W. J. Huggins, M. Head-Gordon, and K. B. Whaley, Journal of Chemical Theory and Computation 15, 311 (2019).
- [56] H. R. Grimsley, S. E. Economou, E. Barnes, and N. J. Mayhall, Nature Communications 10, 3007 (2019).
- [57] H. L. Tang, E. Barnes, H. R. Grimsley, N. J. Mayhall, and S. E. Economou, arXiv:1911.10205 (2019).
- [58] Y. Matsuzawa and Y. Kurashige, Journal of Chemical Theory and Computation 16, 944 (2020).
- [59] K. Mitarai and K. Fujii, Phys. Rev. Research 1, 013006 (2019).
- [60] The projective measurement of P_b can be performed by applying a unitary gate V which satisfies $V^{\dagger}P_bV = Z_0$, executing the projective measurement of Z_0 and finally applying V^{\dagger} after the projective measurement [59]. Such unitary V can be constructed with $O(\log_2 n)$ depth, where n is the number of qubits. First, we transform the non-identity part of P_b into a product of Z gates by using H gates and $S^{\dagger}H$ gates (note that $H \cdot X \cdot H = Z, HS^{\dagger} \cdot Y \cdot HS = Z$). Then CNOT gates are applied to make Z_iZ_j into Z_i by using the equality $\text{CNOT}_{j,i} \cdot Z_iZ_j \cdot \text{CNOT}_{j,i} = Z_i$. Therefore, the depth of quantum gates needed is at most $1 + 2\log_2 n$.
- [61] D.-B. Zhang and T. Yin, arXiv:1910.14030 (2019).
- [62] T. Fukui, Y. Hatsugai, and H. Suzuki, Journal of the Physical Society of Japan 74, 1674 (2005).
- [63] P. Virtanen, R. Gommers, T. E. Oliphant, M. Haberland, T. Reddy, D. Cournapeau, E. Burovski, P. Peterson, W. Weckesser, J. Bright, S. J. van der Walt, M. Brett, J. Wilson, K. J. Millman, N. Mayorov, A. R. J. Nelson, E. Jones, R. Kern, E. Larson, C. J. Carey, İ. Polat, Y. Feng, E. W. Moore, J. VanderPlas, D. Laxalde,

- J. Perktold, R. Cimrman, I. Henriksen, E. A. Quintero, C. R. Harris, A. M. Archibald, A. H. Ribeiro, F. Pedregosa, P. van Mulbregt, A. Vijaykumar, A. P. Bardelli, A. Rothberg, A. Hilboll, A. Kloeckner, A. Scopatz, A. Lee, A. Rokem, C. N. Woods, C. Fulton, C. Masson, C. Häggström, C. Fitzgerald, D. A. Nicholson, D. R. Hagen, D. V. Pasechnik, E. Olivetti, E. Martin, E. Wieser, F. Silva, F. Lenders, F. Wilhelm, G. Young, G. A. Price, G.-L. Ingold, G. E. Allen, G. R. Lee, H. Audren, I. Probst, J. P. Dietrich, J. Silterra, J. T. Webber, J. Slavič, J. Nothman, J. Buchner, J. Kulick, J. L. Schönberger, J. de Miranda Cardoso, J. Reimer, J. Harrington, J. L. C. Rodríguez, J. Nunez-Iglesias, J. Kuczynski, K. Tritz, M. Thoma, M. Newville, M. Kümmerer, M. Bolingbroke, M. Tartre, M. Pak, N. J. Smith, N. Nowaczyk, N. Shebanov, O. Pavlyk, P. A. Brodtkorb, P. Lee, R. T. McGibbon, R. Feldbauer, S. Lewis, S. Tygier, S. Sievert, S. Vigna, S. Peterson, S. More, T. Pudlik, T. Oshima, T. J. Pingel, T. P. Robitaille, T. Spura, T. R. Jones, T. Cera, T. Leslie, T. Zito, T. Krauss, U. Upadhyay, Y. O. Halchenko, Y. Vázquez-Baeza, and S. . . Contributors, Nature Methods (2020), 10.1038/s41592-019 - 0686 - 2.
- [64] "Qiskit," (2020), https://github.com/Qiskit.
- [65] H. J. Werner and W. Meyer, The Journal of Chemical Physics 74, 5802 (1981).
- [66] C. W. Bauschlicher and S. R. Langhoff, The Journal of Chemical Physics 89, 4246 (1988).
- [67] A. D. Bandrauk and J. M. Gauthier, Journal of Physical Chemistry 93, 7552 (1989).
- [68] A. D. Bandrauk and J.-M. Gauthier, J. Opt. Soc. Am. B 7, 1420 (1990).
- [69] Q. Sun, J. Yang, and G. K.-L. Chan, Chemical Physics Letters 683, 291 (2017).
- [70] K. Temme, S. Bravyi, and J. M. Gambetta, Physical review letters 119, 180509 (2017).
- [71] S. Endo, S. C. Benjamin, and Y. Li, Physical Review X 8, 031027 (2018).
- [72] J. C. Tully and R. K. Preston, The Journal of Chemical Physics 55, 562 (1971).
- [73] S. Mai, M. Richter, M. Heindl, M. F. S. J. Menger, A. Atkins, M. Ruckenbauer, F. Plasser, L. M. Ibele, S. Kropf, M. Oppel, P. Marquetand, and L. González, "Sharc2.1: Surface hopping including arbitrary couplings—program package for non-adiabatic dynamics," sharc-md.org (2019).
- [74] M. Richter, P. Marquetand, J. González-Vázquez, I. Sola, and L. González, J. Chem. Theory Comput. 7, 1253 (2011).
- [75] S. Mai, P. Marquetand, and L. González, WIREs Comput. Mol. Sci. 8, e1370 (2018).
- [76] M. Motta, E. Ye, J. R. McClean, Z. Li, A. J. Minnich, R. Babbush, and G. K. Chan, arXiv:1808.02625 (2018).
- [77] W. J. Huggins, J. McClean, N. Rubin, Z. Jiang, N. Wiebe, K. B. Whaley, and R. Babbush, arXiv:1907.13117 (2019).
- [78] S. B. Bravyi and A. Y. Kitaev, Annals of Physics 298, 210 (2002).
- [79] J. T. Seeley, M. J. Richard, and P. J. Love, The Journal of Chemical Physics 137, 224109 (2012), https://doi.org/10.1063/1.4768229.
- [80] S. Bravyi, J. M. Gambetta, A. Mezzacapo, and K. Temme, arXiv:1701.08213 (2017).

- [81] Q. Sun, T. C. Berkelbach, N. S. Blunt, G. H. Booth, S. Guo, Z. Li, J. Liu, J. D. McClain, E. R. Sayfutyarova, S. Sharma, S. Wouters, and G. K. Chan, "Pyscf: the python-based simulations of chemistry framework," (2017).
- [82] J. R. McClean, N. C. Rubin, K. J. Sung, I. D. Kivlichan, X. Bonet-Monroig, Y. Cao, C. Dai, E. S. Fried, C. Gidney, B. Gimby, P. Gokhale, T. Häner, T. Hardikar, V. Havlíček, O. Higgott, C. Huang, J. Izaac, Z. Jiang, X. Liu, S. McArdle, M. Neeley, T. O'Brien, B. O'Gorman, I. Ozfidan, M. D. Radin, J. Romero, N. P. D. Sawaya, B. Senjean, K. Setia, S. Sim, D. S. Steiger, M. Steudtner, Q. Sun, W. Sun, D. Wang, F. Zhang, and R. Babbush, Quantum Science and Technology 5, 034014 (2020).
- [83] W. Hoeffding, Journal of the American Statistical Association 58, 13 (1963).

Supplemental Material

In Supplemental Material, we demonstrate our methods for calculating the NACs, the DBOC, and Berry's phase by numerical simulations. Regarding the NACs, we consider the different electronic states of the hydrogen molecules. For the DBOC, we also take the electronic state of the hydrogen molecules. As for Berry's phase, we take a simple 2-site spin model with a "twist" parameter where Berry's phase is quantized. In these cases, numerical simulations in our method exhibit agreement with the values obtained by numerical differentiation or by solving the model. In addition, we can see the shift of the equilibrium distance by adding the DBOC to the potential energy curve obtained by the VQE [47]. These results further validates our methods proposed in the main text.

1. NACs of the hydrogen molecule

In the numerical simulation of the NACs and the DBOC, the electronic Hamiltonians of the hydrogen molecules are prepared in bond lengths from $0.5\mathring{A}$ to $2.0\mathring{A}$ with the interval of $0.1\mathring{A}$. Furthermore, we arrange the electronic Hamiltonian around the equilibrium point from $0.7320\mathring{A}$ to $0.7350\mathring{A}$ fine enough to see the shift of the equilibrium distance with the interval of $0.0001\mathring{A}$. We perform the standard Hartree-Fock calculation by employing STO-3G minimal basis set and compute the fermionic second-quantized Hamiltonian [2, 3] with open-source libraries PySCF [81] and OpenFermion [82]. The Hamiltonians are mapped to the sum of the Pauli operators (qubit Hamiltonians) by the Jordan-Wigner transformation.

The SSVQE algorithm for the qubit Hamiltonians is executed with an ansatz consisting of SO(4) gates [17] shown in Fig. S1. This ansatz gives real-valued wavefunctions for any parameters $\vec{\theta}$. To obtain charge-neutral and spin-singlet eigenstates, we add penalty terms containing the total particle number operator \hat{N} and the total spin squared operator \hat{S}^2 to the Hamiltonian whose expectation value is to be minimized. The cost function is

$$\mathcal{L}'(\vec{\theta}) = \sum_{i=0}^{M-1} w_i \left\langle \psi_i \middle| U^{\dagger}(\vec{\theta}) H' U(\vec{\theta}) \middle| \psi_i \right\rangle,$$

$$H' = H(\vec{R}) + \beta_S \hat{S}^2 + \beta_N (\hat{N} - N_0)^2,$$
(S1)

where $N_0=2$ is the number of electrons and $\beta_S=\beta_N=10$ are the penalty coefficients. We choose M=3 and obtain the singlet ground state for i=0 and another electronic state for i=2 which has a non-zero value of NACs between the ground state (i.e., having the same symmetry as the ground state). The reference states and the weights are taken as $|\psi_0\rangle=|0001\rangle$, $|\psi_1\rangle=|0011\rangle$, $|\psi_2\rangle=|0101\rangle$ and $w_0=3, w_1=2, w_2=1$. The circuit-parameters $\vec{\theta}$ are optimized by the BFGS algorithm implemented in Scipy library [63]. All simulations are run by the high-speed quantum circuit simulator Qulacs (https://www.github.com/qulacs/qulacs).

The results of the numerical calculation are shown in Fig. S2. We calculate the 1-NAC d_{02} and 2-NAC D_{02} between the ground state i=0 (S_0 state) and the excited state i=2 (S_2 state) as well as the DBOC of the ground state (S_0 state). The results are in agreement with the values computed by numerical differentiation of the full configuration interaction (Full-CI) results based on the definition of the NACs (Eq. (1) and Eq. (2) in the main text). In addition, the result shown in the right bottom panel of Fig. S2 exhibits the shift of the equilibrium distance from 0.7349\AA to 0.7348\AA by considering the DBOC based on Eq. (18) when k=l=0.

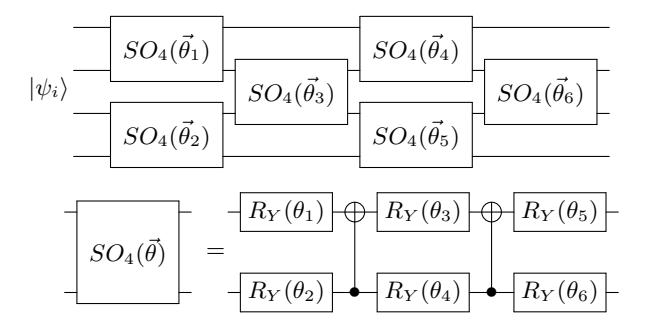


FIG. S1. Ansatz quantum circuit for the VQE of the hydrogen molecule [17]. Each $\vec{\theta}$ has six parameters, and $R_Y(\theta) = e^{-i\frac{\theta}{2}Y}$. The total number of parameters is 36.

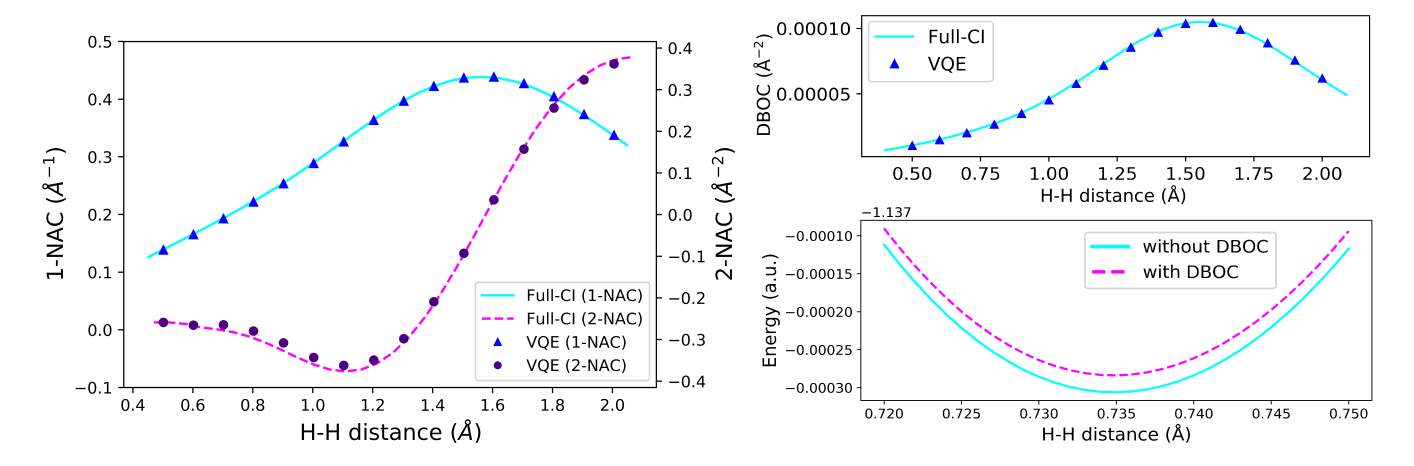


FIG. S2. (left) Numerical results of calculating the 1-NAC d_{02} and 2-NAC D_{02} between S_0 state and S_2 state of the hydrogen molecule in bond lengths from $0.5\mathring{A}$ to $2.0\mathring{A}$ with the interval of $0.1\mathring{A}$. (right top) Numerical results of calculating the DBOC of S_0 state of the hydrogen molecule from $0.5\mathring{A}$ to $2.0\mathring{A}$ with the interval of $0.1\mathring{A}$. (right bottom) Numerical results of calculating potential energy curves by the VQE around the equilibrium distance of the hydrogen molecule without the DBOC (solid line) and with the DBOC (dashed line) from $0.7320\mathring{A}$ to $0.7350\mathring{A}$ with the interval of $0.0001\mathring{A}$. Including the DBOC shifts the equilibrium distance from $0.7349\mathring{A}$ to $0.7348\mathring{A}$. We note that Full-CI represents the values obtained by numerical differentiation of the Full-CI results.

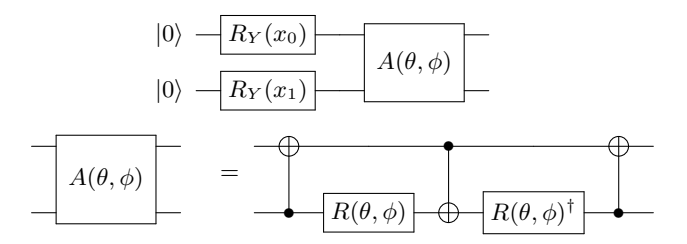


FIG. S3. (top) Ansatz quantum circuit to find the ground state of Eq. (S2). It contains four parameters (x_0, x_1, θ, ϕ) to be optimized. (bottom) Definition of the particle-number-preserving gate $A(\theta, \phi)$ [54]. We define $R(\theta, \phi)$ as $R(\theta, \phi) = R_Y(\theta + \pi/2)R_Z(\phi + \pi)$, where $R_Y(\theta) = e^{i\theta Y/2}$ and $R_Z(\phi) = e^{i\phi Z/2}$.

2. Berry's phase of twisted 2-spin model

To demonstrate our method for Berry's phase, we use a two-site spin-1/2 model with a twist. The Hamiltonian is defined as

$$H_{\Delta}(\rho) = -\frac{1}{2} \left(e^{-i\rho} S_0^+ S_1^- + e^{i\rho} S_0^- S_1^+ \right) + \Delta S_0^z S_1^z, \tag{S2}$$

where $S_i^{\pm} = \frac{1}{2}(X_i \pm Y_i), S_i^z = \frac{1}{2}Z_i$, and ρ is a twist angle. Δ is the parameter determines type and strength of the interaction between spins. The ground state for $-1 < \Delta$ of this model is

$$|\chi_0(\rho)\rangle = \frac{1}{\sqrt{2}} \left(|01\rangle + e^{i\rho} |10\rangle \right),$$
 (S3)

while for $\Delta < -1$ it is degenerate as

$$|\chi_0(\rho)\rangle = |00\rangle, |11\rangle. \tag{S4}$$

Since $H(\rho = 0) = H(\rho = 2\pi)$, we can consider Berry's phase $\Pi_{\mathcal{C}}$ associated to the closed path \mathcal{C} from $\rho = 0$ to $\rho = 2\pi$. From the exact expression of the ground state above, the analytical values of $\Pi_{\mathcal{C}}$ can be calculate as $\Pi_{\mathcal{C}} = \pi$ for $-1 < \Delta$ and $\Pi_{\mathcal{C}} = 0$ for $\Delta < -1$. Berry's phase $\Pi_{\mathcal{C}}$, in this case, is called the local Z_2 Berry's phase and known to detect the topological nature of the ground state of quantum many-body systems [38, 39].

We perform the VQE for the model (S2) with the ansatz depicted in Fig. S3. Again, the BFGS algorithm implemented in Scipy library [63] is used and all quantum circuit simulations are run by Qulacs in the noiseless case. We discretize

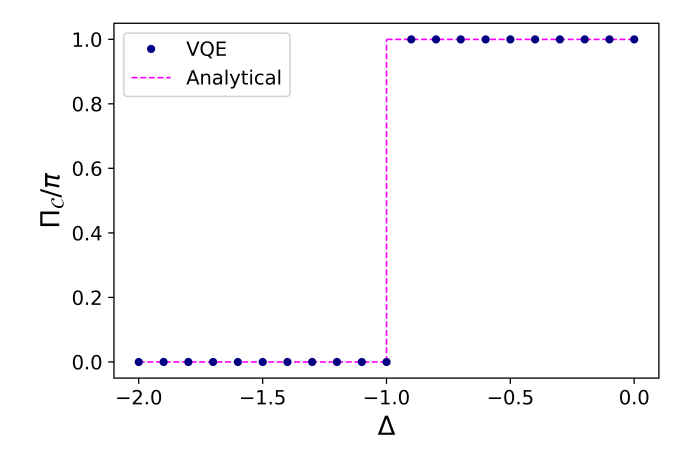


FIG. S4. Numerical results of Berry's phase $\Pi_{\mathcal{C}}$ of the model (S2) based on Eq. (28) for the path $\rho = 0 \to 2\pi$ (dots). The analytical values of the model (S2) (dashed line). We note that the numerical result when $\Delta = -1.0$ is unstable because of the degeneracy of the ground state.

the path from $\rho = 0$ as $\rho = 2\pi$ into 100 points uniformly and run the VQE at each point. The first term of Eq. (28) is calculated by the summation (30) and the phase difference $\Theta_{\rm t} - \Theta_{\rm s}$ in Eq. (28) is evaluated by the Hadamard test in Fig. 2.

The result is shown in Fig. S4. The value of Berry's phase $\Pi_{\mathcal{C}}$ exhibits the sharp transition reflecting the change of the ground state. These results illustrate the validity of our method to calculate Berry's phase by the VQE.